



Petrogenesis of the early Cretaceous Funiushan granites on the southern margin of the North China Craton: Implications for the Mesozoic geological evolution



Xin-Yu Gao^a, Tai-Ping Zhao^{a,*}, Wei-Terry Chen^b

^a Key Laboratory of Mineralogy and Metallogeny, Guangzhou Institute of Geochemistry, Chinese Academy of Sciences, Guangzhou 510640, China

^b Department of Earth Sciences, University of Hong Kong, Hong Kong, China

ARTICLE INFO

Article history:

Received 8 April 2014

Received in revised form 29 July 2014

Accepted 30 July 2014

Available online 8 August 2014

Keywords:

Early Cretaceous granite

Geochemistry

Petrogenesis

North China Craton

ABSTRACT

Late Mesozoic granitoids are ubiquitous in the southern margin of the North China Craton and are keys to the understanding of the Mesozoic geological evolution. The early Cretaceous Funiushan granitic pluton in the southern margin of the North China Craton is composed of porphyritic biotite monzogranites. Rocks from the Funiushan pluton have high SiO₂ (64.45–73.98 wt.%), Na₂O (3.19–4.67 wt.%) and K₂O (3.76–7.95 wt.%) and low MgO (0.11–1.34 wt.%). They are enriched in Rb, Ba, Th, U and LREE ((La/Yb)_N = 9.63–45.0), and depleted in Nb, Ta, Ti and P, and have negative Eu anomalies (Eu/Eu⁺ = 0.29–0.72). This geochemical feature is similar to those of typical I-type granites. Zircons from the granites were dated using LA-ICP-MS and SIMS, and yielded ²⁰⁶Pb/²³⁸U ages of 115–131 Ma. They have ε_{Hf(t)} values mainly vary from -17.7 to +0.9 and T_{DM}^C ages mainly from 2301 to 1118 Ma. Whole rock ε_{Nd(t)} values range from -20.3 to -9.6 and T_{DM} ages from 1.49 to 2.29 Ga, indicating that the magma was produced by partial melting of the Neoarchean to Paleoproterozoic crustal rocks, as represented by the Taihua Group basement rocks, with minor involvement of mantle-derived melts. The Funiushan pluton is considered to have been formed through a strong crust-mantle interaction process under a low pressure condition in an extensional setting, due to the lithospheric thinning caused by westward subduction of the Paleo-Pacific oceanic crust.

© 2014 Elsevier Ltd. All rights reserved.

1. Introduction

The North China Craton (NCC) underwent craton destruction and lithospheric thinning during the late Mesozoic, accompanied by extensive magmatic activity and increased surface heat flux, led to large-scale tectonic extension (e.g. Xu, 2001; Xu et al., 2004; Gao et al., 2004; Wu et al., 2005a; Guo et al., 2013; Li et al., 2013). The ancient subcontinental lithosphere mantle of the NCC was replaced by hot, thin and relatively fresh juvenile lithosphere mantle (e.g. Zheng et al., 2007; Zhang, 2012; Zhang et al., 2013). It is estimated that more than 100 km of the ancient lithosphere may have been destroyed and removed beneath the NCC (e.g. Zhai and Santosh, 2013; Li and Santosh, 2014). The southern margin of the NCC records intense tectonic–magmatic activity during the late Mesozoic, with development of voluminous felsic igneous rocks which are spatially and genetically associated with many world-class Au and Mo ore deposits (e.g. Mao et al., 2008; Chen et al., 2009; Li et al., 2012a). The links among the contemporaneously

occurrence of the granites, metallogeny and lithospheric thinning in the southern margin of the NCC are important to evaluate the geodynamics of craton destruction.

The origin of the late Mesozoic granites along the southern margin of the NCC has been extensively investigated in the past two decades (e.g. Mao et al., 2008, 2010; Li et al., 2012a). They were considered to be produced by partial melting of the NCC ancient crystalline basement (e.g. Guo et al., 2009; Gao et al., 2010; Ding et al., 2011; Hu et al., 2012; Li et al., 2012b; Zhao et al., 2012), or the subducted continental crust of the Yangtze Craton (e.g. Bao et al., 2014). Nevertheless, it remains unclear if the mantle-derived components were involved in the petrogenesis of these granitic intrusions, and to what extent basaltic melts are required (e.g. Hu et al., 2012; Li et al., 2012b; Zhao et al., 2012).

On the other hand, precise formation ages of the granites and their geodynamic background remains unclear. Some of the researchers suggest that the Late Jurassic to Early Cretaceous granites along the southern margin of the NCC formed in a post-collisional extensional setting in response to the collapse of the Qinling Orogenic Belt (QOB) (Hu et al., 1990; Chen et al., 2000), whereas the other think that their generation were formed in a

* Corresponding author. Tel.: +86 20 85290231; fax: +86 20 85290130.

E-mail address: tpzhao@gig.ac.cn (T.-P. Zhao).

lithosphere thinning environment resulted from subduction of the Paleo-Pacific Plate (Sun et al., 2007; Wu et al., 2008; Mao et al., 2010; Li et al., 2012a).

The Funiushan granitic pluton is located at the Funiushan area of the southern margin of the NCC, adjoining the Qinling micro-continent. In late 1980s, the pluton was dated at 613–97.4 Ma (K-Ar and Ar⁴⁰-Ar³⁹) (Wang and Lu, 1998) and therefore was suggested to be formed in the Early Cretaceous (Lu, 1995). It was also regarded as Neoproterozoic migmatitic granites according to their deformation textures (Zhang and Lu, 1990; HIGS, 2002). This study presents newly obtained zircon U-Pb and Hf isotope data, major and trace elements, and whole-rock Sr-Nd isotopes for the Funiushan granitic pluton. Based on the geochemical data, we investigated its petrogenesis and discussed the Mesozoic tectonic framework in the region. Our results may be valuable for understanding the Mesozoic giant mineralization and geological evolution of the southern margin of the NCC.

2. Geological background and field occurrence

The QOB separated is located between the NCC and Yangtze Craton (YZC) (Fig. 1A; Zhang et al., 2001). It comprises three units, including the southern margin of the NCC, the Qinling

micro-continent, and the north margin of the YZC (Fig. 1A). The belt underwent multi-stage tectono-magmatic thermal events from Archaean-Proterozoic to Mesozoic (Zhang et al., 2001; Ratschbacher et al., 2003; Dong et al., 2011; Wu and Zheng, 2013; Li et al., 2013; Zheng et al., 2013).

The southern margin of the NCC is bounded by the Sanmenxia-Lushan Fault to the north and the Luonan – Luanchuan Fault to the south (Fig. 1B), and consists mainly of a Neoarchean – Paleoproterozoic basement rocks (2.26–2.84 Ga; Kröner et al., 1988; Wan et al., 2006; Xu et al., 2009a) that is unconformably overlain by Proterozoic volcanic and sedimentary sequences. The basement is denominated by the Taihua Group that is composed of amphibolite to granulite facies metamorphic rocks. Proterozoic strata consist mainly of mafic to felsic volcanic rocks with minor sedimentary rocks, typically represented by the 1.75–1.78 Ga Xiong'er Group (Zhao et al., 2004a, 2009) and the Meso-Neoproterozoic Guandaokou and Luanchuan Group. Since the earliest Cretaceous, the lacustrine or alluvial sediments began to deposit in the southern margin of the NCC. Magmatic activity is extensive in this area. Pre-Mesozoic granites mainly consists of Neoarchean tonalite-trondhjemite-granodiorite (TTG) rocks, Mesoproterozoic and Neoproterozoic alkaline granites. The late Mesozoic magmatic activity produced voluminous acid intrusive rocks and

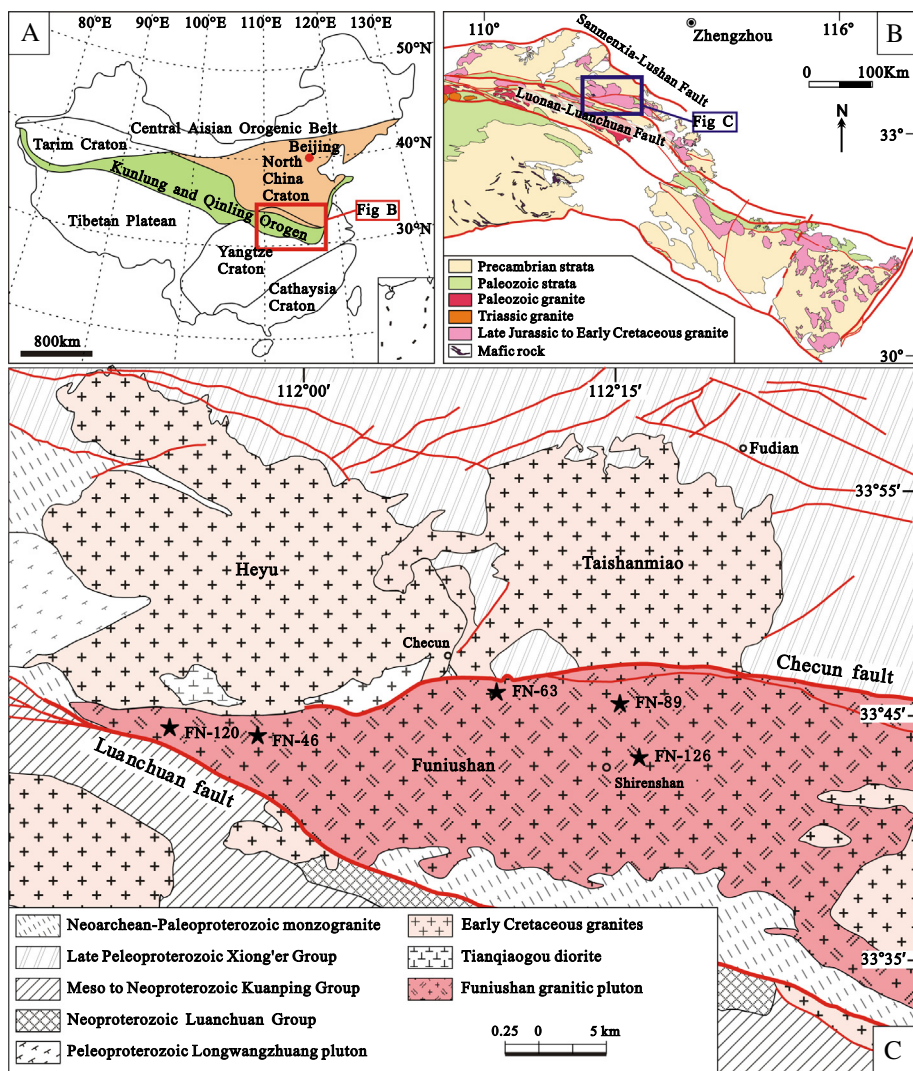


Fig. 1. Geological map in Waifangshan area, southern margin of the North China Craton (NCC). (A) Simplified tectonic map of China showing major tectonic phases surrounding the North China Craton and the location of the Qinling Orogen Belt. (B) Geological map of the Qinling Orogen Belt (modified from Zhang et al., 1996). (C) Geological map of the Funiushan pluton.

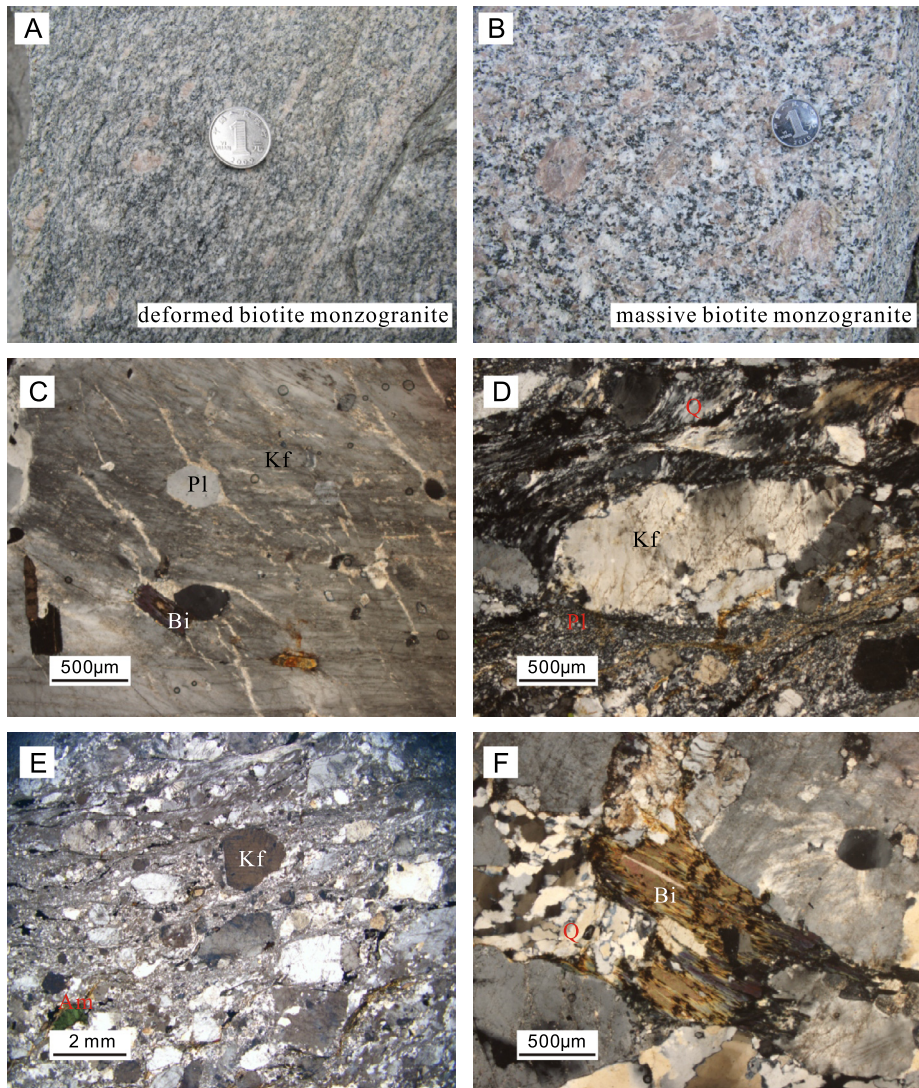


Fig. 2. Field geological observation and petrography: (A) deformed biotite monzogranite with K-feldspar megacrysts; (B) porphyritic biotite monzogranite; (C) quartz, plagioclase and biotite mineral in the perthitic K-feldspar megaphenocrysts; (D) augen structure, caused by sliding and rotating of feldspar megacrysts, and growth of quartz in a pressure shadow; (E) relics of porphyritic texture. The fragmented and dynamically recrystallized groundmass minerals, including micas and quartz bend around preserved relic porphyritic feldspar crystals; (F) corroded or sheared biotite, fragmentation of quartz and recrystallized polygonal quartz. Quartz (Q), K-feldspar (Kf), plagioclase (Pl), biotite (Bi), amphibole (Am).

subvolcanics (Mao et al., 2010) that affected the entire southern margin of the NCC.

The Funiushan pluton on the southern margin of the NCC is a composite body covering an area of 650 km² (Fig. 1C). It intruded the Neoarchean–Paleoproterozoic gneissic monzogranites (zircon U–Pb age 2486 ± 43 Ma; Zhang et al., 1994) in the south and separated from the volcanic rocks of the Xiong'er Group, the early Cretaceous Heyu adakitic granites and the Taishanmiao highly fractionated I-type granites to the north by the Checun fault, and from the Qinling micro-continents to the south by the Luanchuan fault (Fig. 1C). The Funiushan granites contain abundant xenoliths of the basement rocks, most of which are banded and massive amphibolites. The xenoliths are rounded or irregular in shape, ranging from few centimeters to several meters in size, and have sharp or blurred boundaries with their host rocks.

3. Petrography

Rocks from the Funiushan pluton are mainly of coarse to fine-grained porphyritic biotite monzogranites. They consist of

K-feldspar (30–45%), plagioclase (25–35%), quartz (20–30%) and biotite (5–10%), with minor amphibole. K-feldspar occasionally occurs as phenocryst with a size up to 20–30 mm (Fig. 2B). They are mostly subhedral and perthitic, and generally show Carlsbad twinning (Fig. 2C). Platy to prismatic plagioclase is dominantly albite and oligoclase with well-developed polysynthetic twinning. Accessory minerals include opaques (Fe–Ti oxides), allanite, apatite, titanite and zircon.

The outer rims of the Funiushan pluton underwent deformation and metamorphism that are characterized by gneissic structure and mylonitic fabrics (Fig. 1A and C). Mylonitic fabrics are well preserved along its boundaries in contact with the wall-rock or faults. The mylonitic fabric is evident through the strong alignment of fragmented quartz and “augen” of K-feldspar (Fig. 2D and E). K-feldspar presents as relic phenocrysts in the matrix of fine-grained plagioclase, quartz and biotite (Fig. 2E). The fragmented and dynamically recrystallized groundmass minerals including igneous micas flow around the preserved relic quartz and feldspar grains (Fig. 2D). Plagioclase contains large subgrains with straight boundaries. Quartz is elongated and weakly recrystallized and

Table 1

LA-ICP-MS zircon U-Pb data for the Funiushan pluton.

Spots	U (ppm)	Th (ppm)	Th/U	Isotopic ratios						Isotopic ages (Ma)								
				$^{207}\text{Pb}/^{206}\text{Pb}$		σ	$^{207}\text{Pb}/^{235}\text{U}$		σ	$^{206}\text{Pb}/^{238}\text{U}$		σ	$^{207}\text{Pb}/^{206}\text{Pb}$		σ	$^{207}\text{Pb}/^{235}\text{U}$		σ
				Age	σ		Age	σ		Age	σ		Age	σ		Age	σ	
FN-46-01	569	190	0.33	0.05214	0.00171	0.14366	0.00447	0.01999	0.00032	292	73	136	4	128	2			
FN-46-02	320	79	0.25	0.05597	0.00163	0.15366	0.0042	0.01992	0.00031	451	63	145	4	127	2			
FN-46-03	1088	1143	1.05	0.04784	0.00098	0.13583	0.00262	0.02060	0.00029	91	49	129	2	131	2			
FN-46-04	331	118	0.36	0.05060	0.00208	0.14091	0.00557	0.02020	0.00034	223	92	134	5	129	2			
FN-46-05	479	163	0.34	0.05343	0.00201	0.14900	0.00527	0.02023	0.00036	347	83	141	5	129	2			
FN-46-06	514	400	0.78	0.05428	0.00218	0.15281	0.00572	0.02042	0.00039	383	87	144	5	130	2			
FN-46-07	593	255	0.43	0.04685	0.00137	0.13318	0.00369	0.02062	0.00032	41	68	127	3	132	2			
FN-46-08	506	232	0.46	0.04829	0.00192	0.13869	0.00527	0.02083	0.00036	114	91	132	5	133	2			
FN-46-09	756	813	1.08	0.04798	0.00133	0.13728	0.00359	0.02075	0.00032	97	66	131	3	132	2			
FN-46-10	809	602	0.74	0.05055	0.00097	0.14475	0.00263	0.02077	0.00029	220	44	137	2	133	2			
FN-46-11	439	173	0.40	0.04785	0.00177	0.13628	0.00484	0.02066	0.00033	91	86	130	4	132	2			
FN-46-12	428	191	0.45	0.05022	0.00181	0.14251	0.00485	0.02058	0.00035	205	81	135	4	131	2			
FN-46-13	671	439	0.65	0.04725	0.00120	0.13423	0.00325	0.02060	0.00030	61	60	128	3	132	2			
FN-46-14	1831	1927	1.05	0.04885	0.00062	0.14004	0.00172	0.02079	0.00026	141	30	133	2	133	2			
FN-46-15	773	584	0.76	0.04562	0.00116	0.12951	0.00311	0.02059	0.00031	0	38	124	3	131	2			
FN-46-16	546	345	0.63	0.04748	0.00120	0.13635	0.00328	0.02082	0.00030	73	60	130	3	133	2			
FN-46-17	435	209	0.48	0.04696	0.00147	0.13044	0.00393	0.02014	0.00030	47	73	125	4	129	2			
FN-46-18	1149	1093	0.95	0.05056	0.00107	0.14423	0.00288	0.02068	0.00029	221	48	137	3	132	2			
FN-46-19	538	436	0.81	0.05463	0.00259	0.15177	0.00669	0.02014	0.00044	397	102	144	6	129	3			
FN-46-20	934	560	0.60	0.05446	0.00144	0.15313	0.00381	0.02038	0.00031	390	58	145	3	130	2			
FN-46-21	355	199	0.56	0.05299	0.00155	0.14902	0.00404	0.02038	0.00034	328	65	141	4	130	2			
FN-46-22	1017	1128	1.11	0.04773	0.00112	0.13608	0.00302	0.02066	0.00030	85	56	130	3	132	2			
FN-46-23	656	273	0.42	0.04750	0.00196	0.13450	0.00535	0.02052	0.00034	74	96	128	5	131	2			
FN-46-24	376	166	0.44	0.05143	0.00222	0.14389	0.00579	0.02028	0.00041	260	96	137	5	129	3			
FN-63-01	199	273	1.37	0.04560	0.00290	0.11213	0.00684	0.01783	0.00039	0	124	108	6	114	2			
FN-63-02	316	654	2.07	0.06065	0.00236	0.14761	0.00543	0.01765	0.00032	627	82	140	5	113	2			
FN-63-03	400	346	0.87	0.05381	0.00168	0.13302	0.00398	0.01793	0.00028	363	69	127	4	115	2			
FN-63-04	166	386	2.33	0.04862	0.00367	0.12148	0.00893	0.01812	0.00039	130	169	116	8	116	2			
FN-63-05	399	329	0.82	0.08672	0.00299	0.20938	0.00655	0.01751	0.00034	1354	65	193	6	112	2			
FN-63-06	203	328	1.61	0.05426	0.00344	0.13151	0.00791	0.01758	0.00042	382	136	126	7	112	3			
FN-63-07	171	331	1.93	0.05918	0.00411	0.14354	0.00960	0.01759	0.00040	574	144	136	9	112	3			
FN-63-08	257	597	2.33	0.0571	0.00436	0.14106	0.01010	0.01792	0.00053	495	161	134	9	115	3			
FN-63-09	114	216	1.90	0.05312	0.00288	0.12931	0.00666	0.01766	0.00037	334	118	124	6	113	2			
FN-63-10	169	225	1.33	0.05207	0.00493	0.12650	0.01157	0.01762	0.00049	289	202	121	10	113	3			
FN-63-11	78	123	1.58	0.04535	0.00264	0.11132	0.00613	0.0178	0.00041	0	98	107	6	114	3			
FN-63-12	385	311	0.81	0.05331	0.00166	0.12855	0.00378	0.01749	0.00028	342	69	123	3	112	2			
FN-63-13	228	259	1.14	0.05383	0.00427	0.07094	0.00547	0.00956	0.00021	364	169	70	5	61	1			
FN-63-14	7315	12171	1.66	0.08484	0.00077	0.20766	0.00182	0.01775	0.00022	1312	17	192	2	113	1			
FN-63-15	320	416	1.30	0.05560	0.00199	0.13816	0.00464	0.01802	0.00032	436	78	131	4	115	2			
FN-63-16	151	266	1.77	0.05007	0.00347	0.12279	0.00816	0.01779	0.00042	198	153	118	7	114	3			
FN-63-17	136	227	1.67	0.05039	0.00207	0.12483	0.00481	0.01797	0.00034	213	92	119	4	115	2			
FN-63-18	912	800	0.88	0.04918	0.00140	0.11913	0.00319	0.01757	0.00028	156	65	114	3	112	2			
FN-63-19	699	465	0.67	0.04958	0.00745	0.12107	0.01764	0.01771	0.00069	175	317	116	16	113	4			
FN-63-20	687	623	0.91	0.05691	0.00168	0.14078	0.00387	0.01794	0.00029	488	64	134	3	115	2			
FN-63-21	1182	925	0.78	0.04901	0.00090	0.12110	0.00213	0.01792	0.00024	148	43	116	2	115	2			
FN-63-22	269	286	1.07	0.05275	0.00167	0.12837	0.00382	0.01765	0.00029	318	70	123	3	113	2			
FN-63-23	354	465	1.31	0.05921	0.00279	0.14670	0.00648	0.01797	0.00037	575	99	139	6	115	2			
FN-63-24	913	1324	1.45	0.05048	0.00109	0.12405	0.00253	0.01783	0.00025	217	49	119	2	114	2			
FN-89-01	107	128	1.20	0.10077	0.01107	0.25765	0.02545	0.01855	0.00094	1638	191	233	21	119	6			
FN-89-02	200	310	1.55	0.05725	0.00342	0.14502	0.00823	0.01838	0.00041	501	127	138	7	117	3			
FN-89-03	179	321	1.79	0.07798	0.00554	0.20368	0.01326	0.01895	0.00060	1146	135	188	11	121	4			
FN-89-04	58	93	1.61	0.05111	0.01030	0.13113	0.02602	0.01862	0.00070	246	408	125	23	119	4			
FN-89-05	713	666	0.93	0.05245	0.00248	0.13102	0.00584	0.01813	0.00037	305	104	125	5	116	2			
FN-89-06	324	278	0.86	0.06392	0.00417	0.16468	0.00983	0.01869	0.00055	739	132	155	9	119	3			
FN-89-07	121	204	1.68	0.05431	0.00353	0.13923	0.00871	0.0186	0.00040	384	140	132	8	119	3			
FN-89-08	85	195	2.28	0.07083	0.00574	0.17759	0.01357	0.01819	0.00055	953	158	166	12	116	3			
FN-89-09	175	284	1.62	0.07336	0.00443	0.18356	0.01051	0.01816	0.00042	1024	118	171	9	116	3			
FN-89-10	864	1387	1.60	0.05488	0.00210	0.13877	0.00507	0.01835	0.00031	408	83	132	5	117	2			
FN-89-11	414	418	1.01	0.06387	0.00171	0.15821	0.00394	0.01797	0.00029	737	56	149	3	115	2			
FN-89-12	118	188	1.59	0.06982	0.00480	0.18049	0.01174	0.01876	0.00049	923	135	169	10	120	3			
FN-89-13	182	260	1.43	0.06907	0.00367	0.17412	0.00878	0.01829	0.00039	901	106	163	8	117	2			
FN-89-14	225	199	0.88	0.04877	0.00276	0.12618	0.00686	0.01877	0.00038	137	128	121	6	120	2			
FN-89-15	67	102	1.52	0.08738	0.00581	0.22015	0.01356	0.01828	0.00052	1369	123	202	11	117	3			
FN-89-16	1319	1067	0.81	0.07601	0.00413	0.18867	0.00930	0.01801	0.									

Table 1 (continued)

Spots	U (ppm)	Th (ppm)	Th/U	Isotopic ratios						Isotopic ages (Ma)								
				$^{207}\text{Pb}/^{206}\text{Pb}$		σ	$^{207}\text{Pb}/^{235}\text{U}$		σ	$^{206}\text{Pb}/^{238}\text{U}$		σ	$^{207}\text{Pb}/^{206}\text{Pb}$		σ	$^{207}\text{Pb}/^{235}\text{U}$		σ
				Age	σ		Age	σ		Age	σ		Age	σ		Age	σ	
FN-126-2	102	153	1.50	0.05585	0.00268	0.13318	0.00566	0.01730	0.00044	446	103	127	5	111	3			
FN-126-3	95	184	1.94	0.05108	0.00456	0.12220	0.01044	0.01736	0.00051	244	194	117	9	111	3			
FN-126-4	460	330	0.72	0.04509	0.00105	0.11139	0.00241	0.01792	0.00027	0	5	107	2	115	2			
FN-126-5	833	637	0.77	0.05652	0.00186	0.1375	0.00414	0.01765	0.00032	472	72	131	4	113	2			
FN-126-6	506	564	1.11	0.05343	0.00200	0.13263	0.00456	0.01801	0.00035	347	82	127	4	115	2			
FN-126-7	494	591	1.20	0.05110	0.00148	0.12458	0.00328	0.01768	0.00031	246	65	119	3	113	2			
FN-126-8	235	442	1.88	0.04592	0.00216	0.11424	0.00485	0.01804	0.00043	0	103	110	4	115	3			
FN-126-9	527	463	0.88	0.05789	0.00157	0.14472	0.00349	0.01813	0.00032	526	59	137	3	116	2			
FN-126-10	186	333	1.79	0.04850	0.00318	0.12011	0.00741	0.01796	0.00046	124	148	115	7	115	3			
FN-126-11	408	625	1.53	0.05316	0.00276	0.12689	0.00602	0.01731	0.00042	336	113	121	5	111	3			
FN-126-12	154	123	0.80	0.05977	0.00237	0.14527	0.00515	0.01762	0.00038	595	84	138	5	113	2			
FN-126-13	89	150	1.68	0.05040	0.00590	0.12718	0.01420	0.01829	0.00069	213	250	122	13	117	4			
FN-126-14	130	142	1.09	0.05630	0.00409	0.14349	0.00929	0.01848	0.00066	463	154	136	8	118	4			
FN-126-15	869	1349	1.55	0.06029	0.00148	0.15188	0.00335	0.01826	0.0003	614	52	144	3	117	2			
FN-126-16	259	611	2.36	0.0549	0.00331	0.13797	0.00746	0.01822	0.00054	408	129	131	7	116	3			
FN-126-17	197	270	1.37	0.06222	0.00522	0.15501	0.01186	0.01806	0.00067	682	170	146	10	115	4			
FN-126-18	282	343	1.22	0.0493	0.00215	0.12048	0.00479	0.01772	0.00039	162	99	116	4	113	2			
FN-126-19	113	138	1.22	0.06388	0.00724	0.15534	0.01624	0.01763	0.00081	738	223	147	14	113	5			
FN-126-20	187	293	1.57	0.05052	0.00197	0.12400	0.00452	0.01779	0.00034	219	88	119	4	114	2			
FN-126-21	511	508	1.00	0.04348	0.00163	0.10954	0.00388	0.01826	0.00032	0	0	106	4	117	2			
FN-126-22	696	687	0.99	0.04800	0.00145	0.11816	0.00334	0.01784	0.00029	98	71	113	3	114	2			
FN-126-23	841	468	0.56	0.05117	0.00120	0.12696	0.00270	0.01798	0.00028	249	53	121	2	115	2			
FN-126-24	379	874	2.31	0.04966	0.00193	0.12512	0.00453	0.01826	0.00035	179	88	120	4	117	2			

occasionally has chessboard-pattern subgrains (Fig. 2D–F). Fig. 2D also shows quartz in a pressure shadow of an augen K-feldspar. Plagioclase and quartz crystals show commonly undulatory extinction. Biotite flakes are well-oriented and parallel to the main foliation (Fig. 2F).

Thirty-three samples were collected from the porphyritic biotite monzogranites and deformed granites of the pluton for further analyses. Five representative samples from each of the pluton were selected for zircon U–Pb dating, including sample FN-46 ($33^{\circ}44'35''\text{N}$, $111^{\circ}57'46''\text{E}$) from mylonitic porphyritic biotite monzogranite, FN-63 ($33^{\circ}46'25''\text{N}$, $112^{\circ}09'25''\text{E}$) from the mylonitic medium-grained biotite monzogranite, FN-89 ($33^{\circ}45'48''\text{N}$, $112^{\circ}15'08''\text{E}$) from porphyritic biotite monzogranite, FN-126 ($33^{\circ}43'32''\text{N}$, $112^{\circ}15'53''\text{E}$) from biotite monzogranite and FN-120 ($33^{\circ}44'35''\text{N}$, $111^{\circ}53'04''\text{E}$) from the mylonitic fine-grained porphyritic biotite monzogranite (Fig. 1c).

4. Analytical results

4.1. Zircon U–Pb dating

Zircon U–Pb dating results are listed in Tables 1 and 2, and are shown in the concordia plots (Fig. 4). Zircons in rocks from the Funiushan intrusion are subhedral to euhedral and are 100–200 μm long with aspect ratios of 2–4. Most zircon grains are transparent, colorless or tawny (Fig. 3). Their Th/U ratios range from 0.07 to 2.36 (mostly > 0.4) (Table 1), indicating a magmatic origin (Belousova et al., 2002).

Twenty-four analyses of the sample FN-46 have $^{206}\text{Pb}/^{238}\text{U}$ ages ranging from 127 to 133 Ma with a weighted mean age of 131 ± 1 Ma (MSWD = 0.7) (Table 1; Fig. 4a). Similarly, except three analyses deviate the Concordia, and the remaining twenty-one analyses from the sample FN-63 yielded U–Pb ages of

Table 2
SIMS zircon U–Pb data for the Funiushan pluton.

Spots	U (ppm)	Th (ppm)	Th/U	Isotopic ratios						Isotopic ages(Ma)								
				$^{207}\text{Pb}/^{206}\text{Pb}$		1σ	$^{207}\text{Pb}/^{235}\text{U}$		1σ	$^{206}\text{Pb}/^{238}\text{U}$		1σ	$^{207}\text{Pb}/^{206}\text{Pb}$		σ	$^{207}\text{Pb}/^{235}\text{U}$		σ
				Age	σ		Age	σ		Age	σ		Age	σ		Age	σ	
FN-120-1	772	437	0.57	0.04834	0.02573	0.12386	0.03007	0.0186	0.0156	116	60	119	3	119	2			
FN-120-2	563	285	0.51	0.04804	0.05108	0.12555	0.05334	0.0190	0.0154	101	117	120	6	121	2			
FN-120-3	412	117	0.28	0.04821	0.03917	0.12113	0.04210	0.0182	0.0154	109	90	116	5	116	2			
FN-120-4	337	176	0.52	0.04849	0.05474	0.12694	0.05713	0.0190	0.0163	123	124	121	7	121	2			
FN-120-5	1093	972	0.89	0.04856	0.02768	0.12928	0.03149	0.0193	0.0150	127	64	123	4	123	2			
FN-120-6	757	52	0.07	0.04805	0.03508	0.12329	0.03818	0.0186	0.0151	102	81	118	4	119	2			
FN-120-7	535	101	0.19	0.04810	0.05019	0.12143	0.05267	0.0183	0.0160	104	115	116	6	117	2			
FN-120-8	592	104	0.17	0.04823	0.04481	0.12412	0.04738	0.0187	0.0154	110	103	119	5	119	2			
FN-120-9	604	258	0.43	0.04750	0.03702	0.12032	0.04006	0.0184	0.0153	74	86	115	4	117	2			
FN-120-10	1014	216	0.21	0.04829	0.02200	0.12558	0.02671	0.0189	0.0151	113	51	120	3	120	2			
FN-120-11	958	233	0.24	0.04766	0.02356	0.12366	0.02805	0.0188	0.0152	82	55	118	3	120	2			
FN-120-12	723	371	0.51	0.05060	0.02891	0.12991	0.03269	0.0186	0.0153	223	66	124	4	119	2			
FN-120-13	731	611	0.84	0.04807	0.05573	0.12323	0.05786	0.0186	0.0156	103	127	118	6	119	2			
FN-120-14	1160	924	0.80	0.04735	0.02958	0.12388	0.03325	0.0190	0.0152	67	69	119	4	121	2			
FN-120-15	1116	342	0.31	0.04842	0.03873	0.12538	0.04162	0.0188	0.0152	120	89	120	5	120	2			
FN-120-16	430	675	1.57	0.04838	0.04591	0.12432	0.04847	0.0186	0.0155	118	105	119	5	119	2			
FN-120-17	1237	844	0.68	0.05190	0.06831	0.13803	0.07002	0.0193	0.0153	281	149	131	9	123	2			
FN-120-18	1181	694	0.59	0.04785	0.06273	0.12395	0.06460	0.0188	0.0154	92	142	119	7	120	2			
FN-120-19	1725	905	0.52	0.04957	0.02857	0.13047	0.03256	0.0191	0.0156	175	65	125	4	122	2			

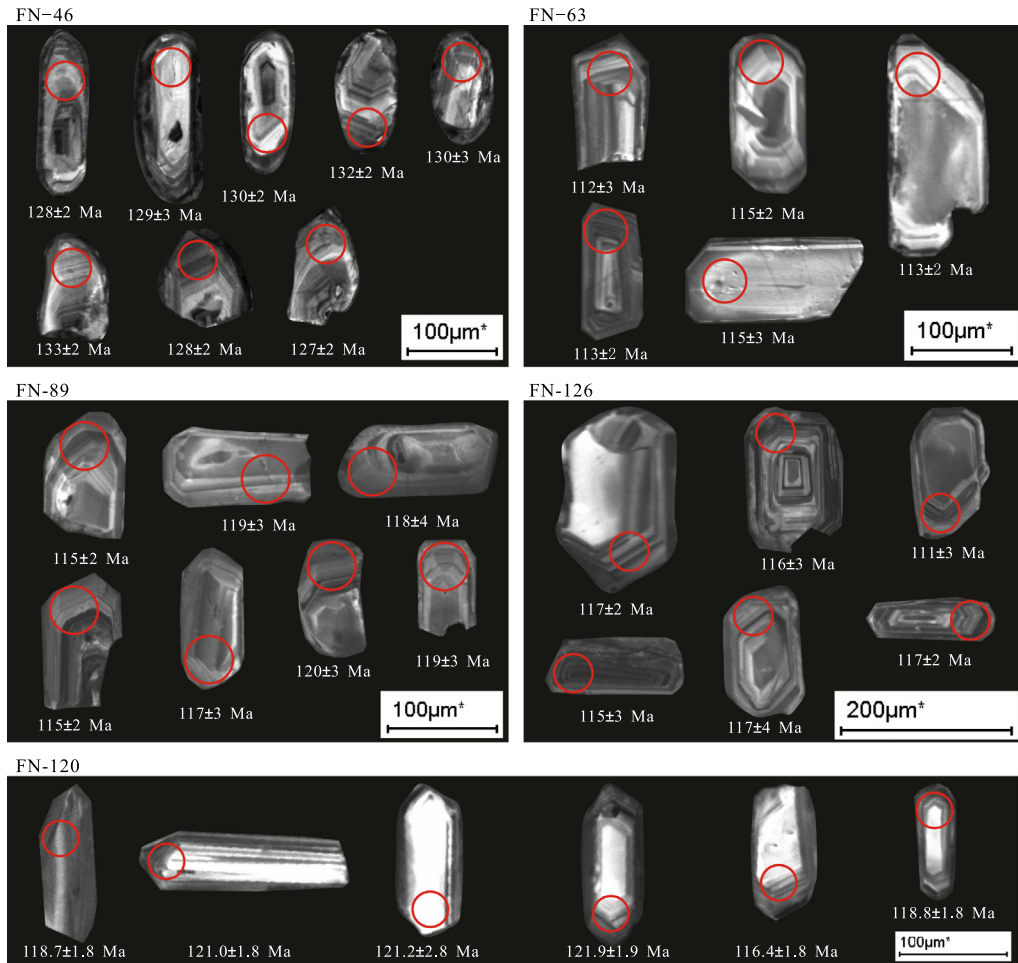


Fig. 3. Representative cathodoluminescence (CL) images of zircon grains from the Funiushan pluton. Red circles show the location of LA-ICP-MS U-Pb and the LA-MC-ICP-MS Hf analyses. (For interpretation of the references to color in this figure legend, the reader is referred to the web version of this article.)

112–116 Ma and a weighted mean age of 115 ± 1 Ma (MSWD = 0.3) (Fig. 4b). Twenty-two analyses on zircons from sample FN-89 have ages ranging from 115 Ma to 122 Ma (Table 1), and yielded a weighted mean age of 117 ± 1 Ma (MSWD = 0.5) (Fig. 4c). Twenty-four analyses on zircons from FN-126 have ages ranging from 111 to 118 Ma (Table 1), and yielded a weighted mean age of 115 ± 1 Ma (MSWD = 0.6) (Fig. 4d). For the sample FN-120, two analyses have high $^{207}\text{Pb}/^{235}\text{U}$ ratios and deviate from the Concordia, the other seventeen analyses have SIMS $^{206}\text{Pb}/^{238}\text{U}$ ages varying from 116 to 123 Ma with a weighted mean age of 120 ± 1 Ma (MSWD = 0.1) (Table 2 and Fig. 4e). The ages of the Funiushan pluton range from 115 to 131 Ma, suggesting that the granitic magmatism may last for a long period of over 10 Mys (Fig. 4f).

4.2. Major and trace elements

Major and trace elements for rocks from the Funiushan pluton are listed in Table 3. The deformed and massive granites have similar geochemical composition. They have high SiO_2 (64.45–73.98 wt.%) and alkalis ($\text{K}_2\text{O} + \text{Na}_2\text{O}$: 8.26–11.29 wt%), and therefore range in composition from granite to alkali granite (Fig. 5h and Table 3). Most samples plot in the high-K calc-alkalic field (Fig. 5g). The granites are metaluminous to peraluminous with A/CNK ratios (molar $\text{Al}_2\text{O}_3/(\text{CaO} + \text{Na}_2\text{O} + \text{K}_2\text{O})$) of 0.96–1.08 (Table 3). They have low MgO contents (0.11–1.34 wt.%) and $\text{Mg}^{\#}$ [$\text{Mg}^{2+}/(\text{Mg}^{2+} + \text{Fe}^{2+}) \times 100$] values (12.8–41.2). In the Harker

diagrams (Fig. 5a–f), TiO_2 , MgO , $\text{Fe}_{2}\text{O}_{3T}$, Al_2O_3 , CaO and P_2O_5 are negatively correlated with SiO_2 .

The granites show LREE enriched and HREE flat distribution Chondrite-normalized REE patterns with $(\text{La/Yb})_{\text{N}}$ ratios of 9.63–45.0 and conspicuous negative Eu anomalies ($\text{Eu/Eu}^* = 0.29$ –0.72) (Table 3 and Fig. 6a). In the primitive mantle-normalized spidergrams (Fig. 6b), they are characterized by enrichment of large ion lithophile elements (LILE) (such as Rb, Sr, Ba, Th and U) and depletion of high field strength elements (HFSE) (such as Nb, Ta, P and Ti).

4.3. Whole rock Sr–Nd isotopes

$^{143}\text{Nd}/^{144}\text{Nd}$ and $^{87}\text{Sr}/^{86}\text{Sr}$ ratios, and Nd model ages for the Funiushan granites are listed in Table 4. Their initial $^{87}\text{Sr}/^{86}\text{Sr}$ range from 0.7063 to 0.7086 and $\varepsilon_{\text{Nd}}(t)$ values from –20.3 to –9.6 (Table 4 and Fig. 7a). The depleted mantle Nd model ages (T_{DM}) are in the range of 1.49–2.29 Ga (Table 4).

4.4. Zircon Lu–Hf isotopic compositions

In situ zircon Hf analyses of four samples (FN-46, FN-63, FN-89 and FN-126) from the Funiushan granites are listed in Table 5 and shown in Figs. 7b and 8a–h. Zircon grains from the four samples have $\varepsilon_{\text{Hf}}(t)$ values ranging from –27.9 to +0.9 (mostly between –17.7 and +0.9), and T_{DM}^{C} ages from 1118 Ma to 2930 Ma (mostly between 1356 Ma and 2301 Ma) (Fig. 8).

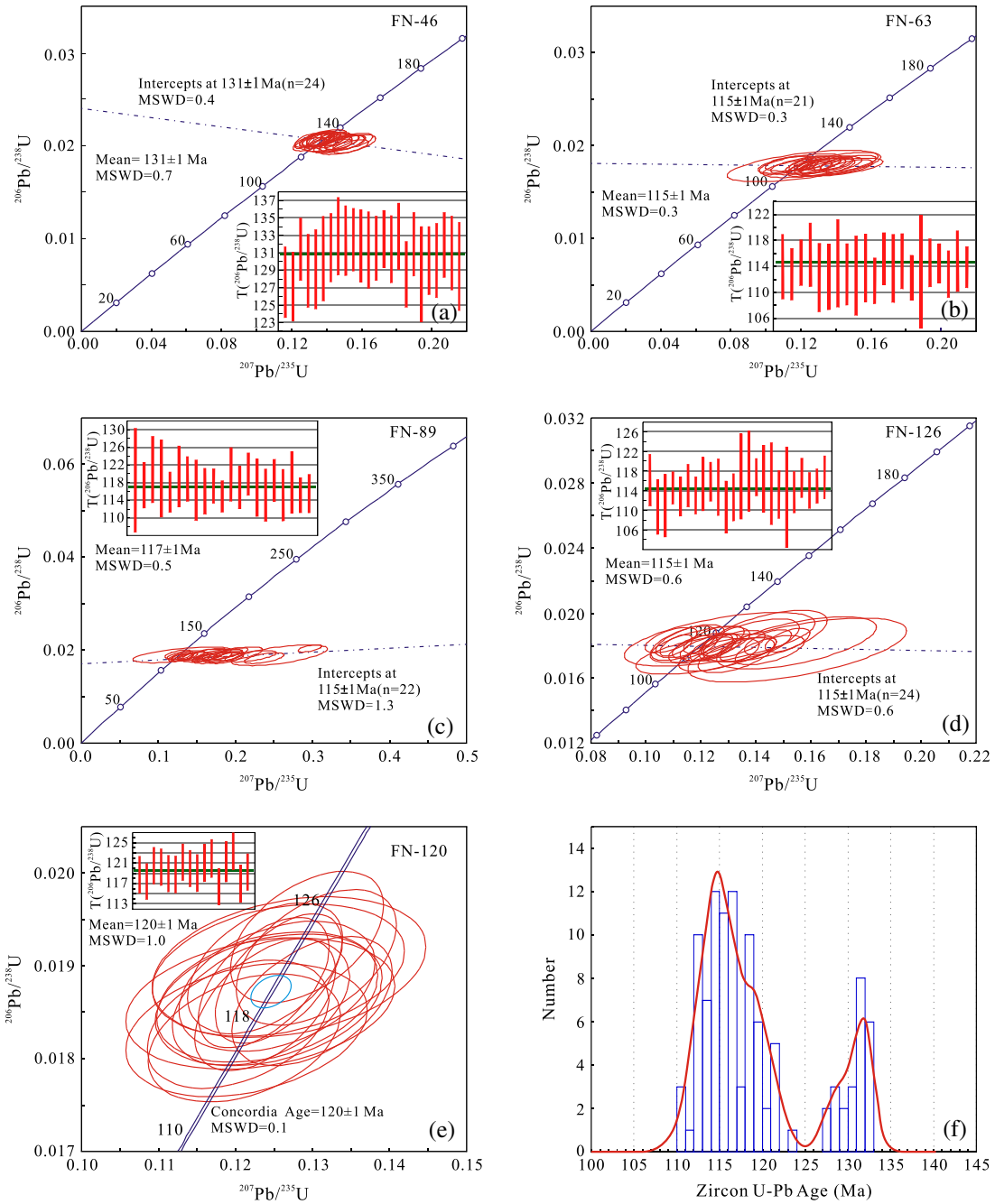


Fig. 4. LA-ICP-MS and SIMS zircon U-Pb concordant plots of the Funiushan pluton.

5. Discussions

5.1. Genetic type and petrogenesis

Rocks from the Funiushan pluton are metaluminous to slightly peraluminous with $A/CNK < 1.1$ and $A/NK > 1.0$. Experiments reveal that apatite can reach saturation in metaluminous and mildly peraluminous magmas ($A/CNK < 1.1$), whereas it is highly soluble in markedly peraluminous melts (Wolf and London, 1994). The Funiushan granites show negative correlation between P_2O_5 and SiO_2 , indicating that they are not S-type granites (Fig. 5f; Chappell, 1999; Li et al., 2004). They contain minor amphibole, but no muscovite and mafic alkaline minerals such as arfvedsonite and riebeckite. They have low contents of Zr (95.4–334 ppm, average 225 ppm) that are lower than the limit of A-type granites

($Zr > 250$ ppm, Whalen et al., 1987). They also have lower FeO_T/MgO ratios (2.99–14.3, average 4.6) than that of A-type granites ($FeO_T/MgO > 10$, Whalen et al., 1987). In addition, zircon saturation temperatures of the granitic magma is estimated to be 694 °C and 830 °C with an average value of 797 °C (Watson and Harrison, 1983), lower than that of A-type granites (King et al., 1997, 2001). Thus, rocks from the Funiushan pluton are classified as I-type series, rather than S-type or A-type granites (Chappell and White, 1992; Chappell, 1999).

Geochemical characteristics of the Funiushan granites, such as enrichment of LREE and flat HREE patterns, significantly negative Eu anomalies, and the depletion in Sr, P, and Ti (Fig. 6), suggest that amphibole and plagioclase were important residual phases in the source region (e.g. Martin et al., 2005). In addition, they have low $(La/Yb)_N$ and Sr/Y ratio, suggesting that their parental magmas

Table 3

Major (wt.%) and trace element concentrations (ppm) of the Funiushan pluton.

Samples	FN-37	FN-43	FN-46	FN-49	FN-54	FN-56	FN-63	FN-67	FN-77	FN-89	FN-95	FN-101	FN-102	FN-103	FN-109	FN-112	FN-120
SiO ₂	73.64	72.69	68.23	70.45	71.64	70.88	71.68	68.54	67.11	65.31	70.05	70.75	71.99	67.06	69.85	73.98	68.62
TiO ₂	0.17	0.18	0.35	0.29	0.23	0.28	0.43	0.25	0.62	0.65	0.30	0.29	0.27	0.39	0.54	0.11	0.61
Al ₂ O ₃	13.77	14.39	16.12	15.26	14.66	15.29	14.35	16.19	15.31	15.83	15.72	14.90	14.47	16.48	14.74	14.08	15.04
Fe ₂ O ₃	1.81	1.53	2.59	2.16	1.79	1.79	2.30	1.71	3.94	4.31	2.03	2.21	1.82	2.71	2.97	1.30	3.70
MnO	0.04	0.02	0.04	0.04	0.03	0.03	0.06	0.05	0.07	0.08	0.03	0.04	0.03	0.05	0.07	0.03	0.07
MgO	0.11	0.23	0.46	0.45	0.33	0.39	0.48	0.39	0.94	1.28	0.43	0.44	0.44	0.58	0.69	0.11	0.84
CaO	0.77	1.12	1.49	1.69	1.23	1.77	1.40	0.73	2.12	2.76	1.67	1.65	1.36	1.79	1.81	1.10	1.69
Na ₂ O	3.96	3.47	4.16	4.11	3.84	3.96	3.19	3.34	3.41	3.84	4.21	4.10	3.29	4.2	3.71	3.76	3.93
K ₂ O	4.83	5.44	5.57	4.68	4.78	4.56	5.08	7.95	5.45	4.82	4.58	4.50	5.25	5.83	5.00	4.76	4.79
P ₂ O ₅	0.03	0.03	0.16	0.14	0.08	0.10	0.11	0.10	0.21	0.24	0.10	0.13	0.08	0.15	0.16	0.03	0.24
LOI	0.40	0.42	0.35	0.25	0.92	0.47	0.44	0.28	0.33	0.42	0.40	0.52	0.53	0.28	0.11	0.27	0.10
Total	99.53	99.52	99.53	99.52	99.53	99.53	99.53	99.53	99.53	99.53	99.52	99.52	99.54	99.53	99.53	99.53	99.53
Mg [#]	12.8	26.3	29.4	32.6	30.1	33.9	32.9	34.9	35.7	40.9	33.0	31.7	36.2	33.4	35	16.0	34.5
ANK	1.17	1.24	1.25	1.29	1.28	1.33	1.34	1.15	1.33	1.37	1.32	1.28	1.30	1.25	1.28	1.24	1.29
ACNK	1.05	1.06	1.03	1.02	1.07	1.04	1.08	1.05	1.00	0.96	1.05	1.02	1.07	1.00	1.00	1.06	1.02
Cs	1.98	1.70	1.79	1.39	0.69	1.79	1.85	5.86	2.93	2.43	0.69	0.66	1.12	0.54	2.16	0.77	0.98
Rb	200	172	136	113	128	132	192	299	166	154	116	104	177	125	180	139	124
Ba	297	1454	2580	1989	1796	1605	771	2107	1369	1354	1531	2315	947	3175	926	674	1394
Th	28.6	74.3	27.4	27.0	25.4	15.8	44.8	18.5	19.8	19.0	22.5	13.6	25.7	24.1	42.6	18.3	19.9
U	12.43	12.64	3.22	2.12	1.65	3.31	5.53	5.15	3.99	3.1	1.91	1.51	3.06	1.48	4.54	2.35	3.10
Nb	53.1	26.8	44.2	34.1	25.5	24.2	39.8	41.5	38.9	28	30	32.9	12.2	39.9	44.1	32.4	31.1
Ta	1.76	1.92	3.5	1.82	0.76	1.82	1.8	2.71	2.08	1.89	2.38	2.15	0.92	2.58	3.10	1.46	2.51
Sr	123	390	789	709	680	603	189	405	351	398	524	750	185	840	265	264	354
Y	30.4	12.5	21.4	13.8	12.9	12.3	34.6	16.4	50.9	34.2	25.4	15.7	22.2	18.1	41.7	15.0	32.8
Zr	302	162	254	207	217	165	260	273	279	266	226	217	226	252	291	109	325
Hf	9.40	4.69	5.84	5.35	6.10	4.74	7.37	8.26	7.78	7.10	6.32	5.91	6.80	6.42	7.92	3.78	8.75
La	61.4	38.6	85.0	67.2	59.5	41.3	81.6	47.0	73.7	73.4	79.6	64.5	54.1	104.3	93.1	22.7	60.5
Ce	112	66.1	141	110	110	73.2	146	83.9	163	134	130	111	102	176	175	42.1	111
Pr	13.2	7.30	16.5	11.4	11.1	8.50	15.6	9.38	19.3	14.9	15.6	12.4	11.8	17.7	18.2	5.09	12.3
Nd	46.1	24.1	53.8	37.3	36	29.4	51.4	32.6	67.2	49.7	54.8	42.1	39.8	57.8	60.8	19.1	44.3
Sm	7.69	3.81	8.62	5.52	5.60	5.23	8.21	5.45	12.24	8.60	10.02	6.96	6.53	8.36	10.09	4.04	7.85
Eu	0.68	0.80	1.60	1.12	1.06	1.11	1.10	0.87	1.54	1.48	1.71	1.34	0.83	1.62	1.57	0.64	1.51
Gd	6.38	2.92	6.07	3.96	3.71	3.82	6.57	4.18	9.55	7.32	7.46	4.94	4.85	5.66	7.88	3.63	6.67
Tb	0.96	0.42	0.82	0.51	0.49	0.49	1.03	0.57	1.51	1.10	1.03	0.67	0.70	0.78	1.29	0.55	1.03
Dy	5.47	2.18	3.97	2.59	2.54	2.39	6.11	2.85	9.02	5.98	5.48	3.32	3.89	3.65	7.27	3.16	5.99
Ho	1.11	0.44	0.74	0.47	0.49	0.46	1.23	0.59	1.90	1.27	1.06	0.59	0.80	0.67	1.54	0.60	1.25
Er	3.25	1.38	2.18	1.37	1.24	1.25	3.74	1.73	5.48	3.55	2.54	1.58	2.38	1.90	4.46	1.60	3.44
Tm	0.46	0.19	0.27	0.17	0.17	0.54	0.24	0.76	0.50	0.31	0.18	0.33	0.22	0.65	0.21	0.52	
Yb	3.23	1.35	1.73	1.21	1.06	1.25	3.84	1.77	4.95	3.32	1.98	1.30	2.31	1.66	4.29	1.28	3.52
Lu	0.49	0.19	0.24	0.17	0.14	0.19	0.58	0.26	0.71	0.5	0.25	0.19	0.34	0.22	0.64	0.18	0.51
ΣREE	293	162	344	257	246	181	363	208	422	340	337	267	253	399	428	120	293
LREE	241	141	307	233	223	159	304	179	337	282	292	238	215	366	359	94.0	238
HREE	51.7	21.5	37.4	24.3	22.8	22.3	58.3	28.6	84.8	57.7	45.5	28.4	37.8	32.9	69.7	26.3	55.8
LREE/HREE	4.66	6.53	8.20	9.60	9.79	7.12	5.22	6.27	3.98	4.89	6.41	8.37	5.67	11.13	5.14	3.57	4.26
(La/Yb) _N	13.6	20.5	35.2	39.9	40.2	23.7	15.2	19.0	10.7	15.9	28.9	35.6	16.8	45.0	15.6	12.7	12.4
δEu = Eu/Eu*	0.29	0.7	0.64	0.70	0.67	0.72	0.44	0.54	0.42	0.56	0.58	0.66	0.43	0.68	0.52	0.50	0.62
T °C	777	702	772	782	694	813	805	794	791	776	786	804	697	784	759	782	816
	FN-124	FN-125	FN-126	FN-127	FN-128	FN-129	FN-136	FN-137	FN-143	FN-153	FN-156	FN-160	FN-161	FN-163	FN-165	FN-183	
SiO ₂	70.8	72.68	67.87	73.33	66.13	71.93	64.45	72.84	71.46	66.78	68.94	71.21	67.27	73.66	67.88	69.40	
TiO ₂	0.29	0.19	0.57	0.15	0.56	0.18	0.66	0.24	0.22	0.50	0.49	0.29	0.35	0.15	0.39	0.27	
Al ₂ O ₃	14.83	14.19	15.15	14.55	15.95	15.12	16.40	14.18	14.75	16.48	14.99	14.92	16.69	14.36	16.13	15.78	
Fe ₂ O ₃	1.92	1.28	3.44	1.16	3.61	1.33	4.45	1.57	1.58	3.05	3.05	1.94	2.25	1.12	2.84	1.96	
MnO	0.04	0.03	0.09	0.03	0.06	0.03	0.12	0.03	0.05	0.05	0.06	0.03	0.04	0.03	0.05	0.04	
MgO	0.38	0.33	1.00	0.19	0.83	0.38	1.34	0.35	0.28	0.74	0.72	0.55	0.63	0.24	0.52	0.44	
CaO	1.41	1.15	1.93	1.07	1.96	1.63	2.83	1.18	1.04	2.18	1.66	1.69	2.43	1.41	1.76	1.71	
Na ₂ O	3.84	3.26	3.75	3.91	3.63	3.81	4.09	3.40	3.65	4.17	3.47	3.70	4.67	3.68	4.28	4.12	
K ₂ O	4.74	5.28	5.16	4.86	6.25	4.67	4.49	5.4	5.47	4.95	5.64	4.83	3.76	4.63	5.22	5.26	
P ₂ O ₅	0.09	0.05	0.2	0.04	0.18	0.07	0.27	0.06	0.07	0.18	0.14	0.08	0.09	0.03	0.17	0.15	
LOI	1.19	1.12	0.38	0.23	0.36	0.39	0.42	0.27	0.97	0.43	0.36	0.29	1.37	0.23	0.29	0.40	
Total	99.53	99.56	99.53	99.53	99.52	99.53	99.53	99.53	99.52	99.52	99.53	99.54	99.53	99.53	99.53	99.53	
Mg [#]	31.6	37.3	40.4	27.9	34.9	40.1	41.2	34.3	29.1	36.1	35.4	39.5	39.5	33.4	29.9	34.5	
ANK	1.29	1.28	1.29	1.24	1.25	1.33	1.42	1.24	1.24	1.35	1.27	1.32	1.42	1.30	1.27	1.27	
ACNK	1.06	1.08	0.99	1.07	0.98	1.06	0.98	1.04	1.07	1.02	1.01	1.04	1.03	1.05	1.01	1.01	
Cs	1.03	1.61	1.77	1.70	1.66	3.73	2.53	1.54	3.74	1.13	1.30	2.20	2.01	1.39	1.98	1.04	
Rb	157	216	195	165	191	231	230	247	133	180	191	144	161	143	156		
Ba	1871	702	962	894	1												

Hf	6.41	4.69	7.51	3.34	8.03	3.82	6.86	5.01	5.13	7.90	8.22	4.33	4.29	3.00	6.81	5.61
La	77.0	49.0	78.5	34.0	99.7	26.6	60.4	40.2	68.7	92.3	112.5	56.4	66.1	31.6	113	71.7
Ce	139	82.9	153	62.0	191	48.6	133	73.1	117	170	207	104	122	55.5	197	117
Pr	15.2	8.75	17.4	6.77	21.1	5.53	15.7	7.56	12.5	18.1	21.3	11.3	13.5	5.67	20.0	12.2
Nd	52.5	28.5	57.9	22.9	70.9	19.5	52.6	25.0	39.7	60.9	67.2	36.1	44.3	17.7	62.9	39.5
Sm	8.48	5.01	9.44	3.72	11.99	3.63	8.86	4.15	5.76	9.36	10.97	5.83	7.04	2.73	8.87	5.62
Eu	1.45	0.64	1.42	0.67	1.52	0.72	1.41	0.61	0.95	1.96	1.36	0.76	1.02	0.49	1.84	1.16
Gd	5.61	3.95	7.68	3.01	10.4	3.25	7.58	3.49	4.48	6.92	9.47	5.02	5.87	2.29	6.93	4.09
Tb	0.79	0.68	1.17	0.41	1.47	0.47	1.06	0.51	0.61	0.95	1.38	0.70	0.83	0.35	0.87	0.54
Dy	3.48	3.90	7.02	2.16	8.44	2.45	6.27	2.85	3.26	4.20	7.71	3.78	4.63	2.06	3.93	2.40
Ho	0.60	0.81	1.45	0.43	1.85	0.49	1.37	0.61	0.63	0.81	1.70	0.85	0.97	0.47	0.74	0.50
Er	1.65	2.36	4.08	1.21	4.78	1.31	4.07	1.88	1.74	2.17	4.68	2.58	2.72	1.44	2.09	1.34
Tm	0.20	0.35	0.62	0.17	0.72	0.19	0.63	0.31	0.26	0.27	0.68	0.37	0.39	0.24	0.26	0.18
Yb	1.37	2.52	4.14	1.18	4.79	1.33	4.50	2.22	1.75	1.77	4.55	2.72	2.56	1.67	1.91	1.24
Lu	0.20	0.39	0.65	0.17	0.64	0.21	0.69	0.34	0.28	0.23	0.63	0.40	0.38	0.29	0.26	0.21
Σ REE	323	212	385	152	479	129	341	183	276	392	497	256	301	138	442	271
LREE	294	175	318	130	396	105	272	151	244	353	421	215	254	114	403	247
HREE	29.5	36.8	67.6	21.7	82.9	24.9	68.8	32	32.2	39.2	76.7	41.8	46.4	23.8	38.5	24.2
LREE/HREE	9.94	4.75	4.70	6.00	4.78	4.21	3.96	4.71	7.59	8.99	5.48	5.14	5.47	4.79	10.47	10.19
(La/Yb) _N	40.3	14.0	13.6	20.7	14.9	14.4	9.60	13.0	28.2	37.3	17.7	14.9	18.6	13.6	42.5	41.3
δ Eu = Eu/Eu [*]	0.60	0.42	0.49	0.6	0.41	0.62	0.51	0.48	0.55	0.71	0.40	0.42	0.47	0.58	0.69	0.71
T °C	825	830	811	828	806	825	803	826	826	812	815	822	813	827	813	816

ACNK = molar Al₂O₃/(CaO + Na₂O + K₂O); ANK = molar Al₂O₃/(Na₂O + K₂O); Mg[#] = Mg²⁺/(Mg²⁺ + Fe²⁺) × 100; δEu = ω(Eu)_N/[(1/2)(ω(Sm)_N + ω(Gd)_N)]; T_{Zr} zircon saturation temperatures (Watson and Harrison (1983)).

were generated under low pressures without garnet residual during the partial melting (e.g. Martin et al., 2005; Klein et al., 2000; Pertermann et al., 2004).

5.2. Nature of the magma source

Felsic rocks may be produced by partial melting of lower crust, or fractioanl crystallization or immiscible separation of mafic magmas (Zhou et al., 2013). The Funiushan granites have low initial $^{87}\text{Sr}/^{86}\text{Sr}$ ratios (0.7063–0.7086), but large variable negative $\varepsilon_{\text{Nd}}(t)$ values (−20.3 to −9.6) and zircon $\varepsilon_{\text{Hf}}(t)$ values (−17.7 to −2.8) (Tables 4 and 5). Their two-stage Nd and Hf model ages range from 1.49 to 2.29 Ga and from 1.36 to 2.30 Ga, respectively. These data suggest that the parental magmas of the Funiushan granites were probably formed by partial melting of Mesoproterozoic to Paleoproterozoic continental crust. The large variations of Sr–Nd–Hf isotopes probably indicate a heterogeneous source (e.g. Kemp et al., 2005; Zhao et al., 2013a).

The widespread Neoproterozoic to Paleoproterozoic Taihua Group basement rocks is the oldest rocks of the southern margin of the NCC. Their amphibolite to granulite facies mafic rocks suggest that they were derived from the middle – lower crust and therefore are the potential source rocks of the Funiushan granites (e.g. Zhao et al., 2013b). Amphibole, clinopyroxene and plagioclase are considered to be major residual minerals in the partial melting. The average composition of amphibolites from the Taihua group is taken to be the source composition. Partition coefficients used in the modeling are carefully selected and listed in Table 6. The modeling results show that low degree (5–20%) melting of the amphibolites with residues of amphibole (~70%) + clinopyroxene (~10%) + plagioclase (~20%) can produce partial melts with trace element abundances and patterns well matching the Funiushan granites (Table 6 and Fig. 10).

However, the majority of dehydration melts derived from amphibolites have high Na₂O and relatively low K₂O concentrations (Beard and Lofgren, 1991), regardless of their degrees of partial melting, differentiate these melts from most of those that formed the high-K calc-alkaline Funiushan granites, indicating that another source member with medium to high K contents is in need (Fig. 9). Moreover, the Funiushan granites have two-stage Hf model ages much younger than that of the Taihua Groups. Their $\varepsilon_{\text{Hf}}(t)$ values are higher than those of the Taihua Group at $t = 120$ Ma (Fig. 7). They also have lower initial $^{87}\text{Sr}/^{86}\text{Sr}$ ratios and higher $\varepsilon_{\text{Nd}}(t)$ values

than those of the Taihua Group (Fig. 7a; Huang and Wu, 1990; Zhang and Li, 1998; Xu et al., 2009a; Ni et al., 2012). These geochemical data suggest that the mantle-derived magmas must have been involved in the petrogenesis of the granites. A simple mixing modeling was taken to address role of the mantle-derived melts in the petrogenesis of the Funiushan granites. The Sr–Nd isotope modeling reveals that more than 20–60% mantle-derived melts are required (Fig. 7a). It suggests that the granitic magmas were produced by partial melting of a mixed lithology containing amphibolite of the Taihua Group underplated by a medium to high K basaltic magma for the latter. In addition, zircons from the 115–120 Ma granites have $\varepsilon_{\text{Hf}}(t)$ values range from −17.5 to 0.9, systematically higher than that of the 131 Ma granites ($\varepsilon_{\text{Hf}}(t) = -27.9$ to −4.3) (Table 5; Figs. 7b and 8). Thus, the younger granites contain more fractions of mantle material than the slightly older ones.

5.3. Geodynamic background

The widespread late Mesozoic granitic rocks in the QOB were generally formed in three episodes (Mao et al., 2008): Late Triassic (233–221 Ma), Late Jurassic to Early Cretaceous (148–138 Ma), and Early to Middle Cretaceous (131–112 Ma). Granites from the southern margin of the NCC are dominated by the late Jurassic to middle Cretaceous (160–110 Ma) high-K calc-alkaline granites (e.g. Gao et al., 2010; Guo et al., 2009; Mao et al., 2010; Hu et al., 2012; Li et al., 2012b; Zhao et al., 2012) which are enriched in Sr, Ba and LREE, and depleted in Y and Yb with crustal isotopic signatures. These adakitic granites form a roughly northwest–southeast trending belt along the southern margin of the NCC and are considered to be produced by partial melting of thickened lower continental crust (e.g. Guo et al., 2009; Hu et al., 2012; Li et al., 2012b; Zhao et al., 2012; Zhu et al., 2012b), suggesting that the crust were thickened before late Jurassic. The Funiushan granites are geochemically different from the adakitic granites. They are coeval with the widespread early Cretaceous granites in the NCC, that were probably formed under lower pressure due to intracontinental extension and lithospheric thinning occurred in the whole eastern China (e.g. Jahn et al., 1999; Zhao et al., 2004b, 2007b; Xie et al., 2006; Yang et al., 2008, 2014; Guo et al., 2013; Tang et al., 2013; Zhai and Santosh, 2013; Goldfarb and Santosh, 2014).

Extensive melting of silicic crust requires large heat flux, which can only be supplied by mantle-derived magmas (e.g. Bird, 1978;

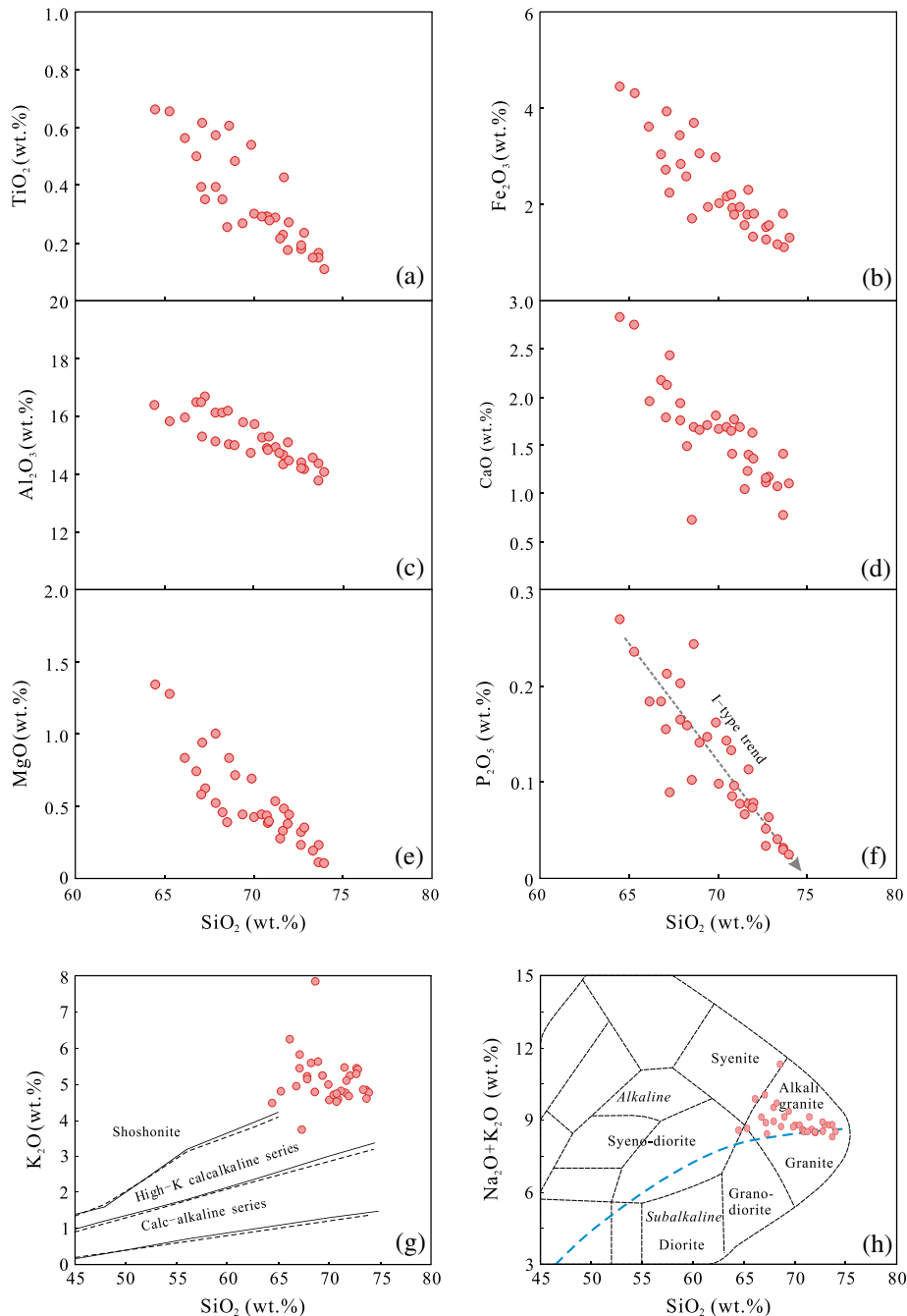


Fig. 5. Major elements vs. SiO_2 plots of the Funiushan pluton. The $\text{Na}_2\text{O} + \text{K}_2\text{O}$ vs. SiO_2 diagrams are from Wilson (1989).

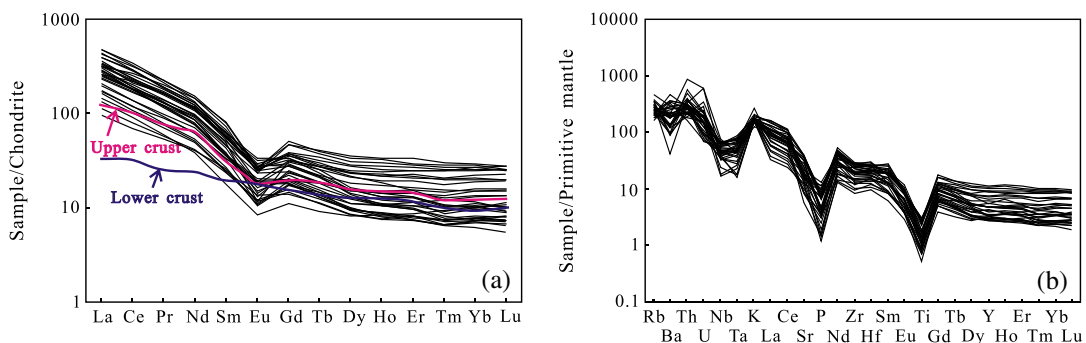


Fig. 6. Chondrite-normalized REE patterns (a) and primitive mantle-normalized trace element (b) diagrams for the Funiushan pluton. The normalization values are from Sun and McDonough (1989); upper and lower continental crust values are from Rudnick and Gao (2003).

Table 4

Whole-rock Sr–Nd isotopic data of the Funiushan pluton.

Sample	$^{87}\text{Rb}/^{86}\text{Sr}$	$^{87}\text{Sr}/^{86}\text{Sr}$	2σ	I_{Sr}	$^{147}\text{Sm}/^{144}\text{Nd}$	$^{143}\text{Nd}/^{144}\text{Nd}$	2σ	$\varepsilon_{\text{Nd}}(t)$	T_{DM} (Ga)	$f_{\text{Sm/Nd}}$
FN-37	4.5928	0.714774	0.000005	0.7070	0.1058	0.511528	0.000004	-20.3	2.29	-0.46
FN-46	0.4869	0.708946	0.000005	0.7080	0.1017	0.511715	0.000004	-16.4	1.95	-0.48
FN-54	0.5317	0.707115	0.000006	0.7063	0.0987	0.511827	0.000003	-14.4	1.75	-0.50
FN-63	2.8694	0.711810	0.000005	0.7072	0.1013	0.512037	0.000003	-10.3	1.51	-0.48
FN-89	1.0929	0.708423	0.000005	0.7066	0.1098	0.512060	0.000004	-10.0	1.60	-0.44
FN-103	0.4203	0.709233	0.000005	0.7085	0.0918	0.511676	0.000004	-17.2	1.84	-0.53
FN-126	1.6105	0.708929	0.000005	0.7063	0.1034	0.512072	0.000004	-9.7	1.49	-0.47
FN-143	1.7662	0.711188	0.000005	0.7083	0.0921	0.511789	0.000004	-15.0	1.70	-0.53
FN-147	0.4687	0.707293	0.000007	0.7065	0.1071	0.512073	0.000004	-9.7	1.54	-0.46
FN-149	0.4759	0.707252	0.000004	0.7065	0.1080	0.512080	0.000003	-9.6	1.54	-0.45
FN-160	1.7291	0.711821	0.000005	0.7086	0.1025	0.511732	0.000004	-16.1	1.94	-0.48
FN-161	0.9437	0.710312	0.000005	0.7086	0.1008	0.511735	0.000004	-16.0	1.91	-0.49

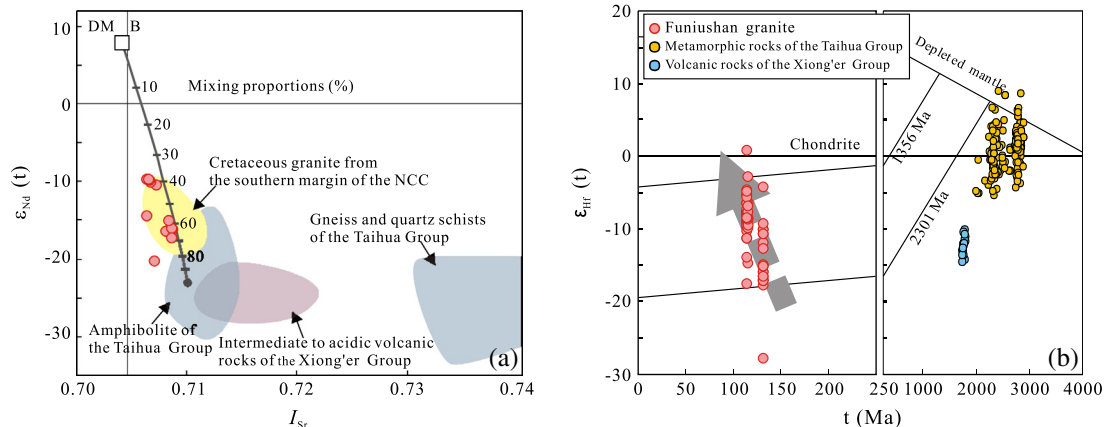


Fig. 7. $\varepsilon_{\text{Nd}}(t)$ vs. I_{Sr} diagram (a) and Zircon Hf isotopic compositions of the Funiushan pluton (b). (a) The $\varepsilon_{\text{Nd}}(t)$ and I_{Sr} values of the Taihua and Xiong'er Group is calculated at $t = 120$ Ma. [amphibolite of Taihua Group: Sr = 388 ppm, $I_{\text{Sr}} = 0.71$, Nd = 26.6 ppm, $\varepsilon_{\text{Nd}}(t = 120) = -23$ (Sr and Nd data using 20% of partial melting of amphibolite of the Taihua Group in Table 6; Huang and Wu, 1990; Ni et al., 2012; Zhang and Li, 1998); gneiss and quartz schists of the Taihua Group (Huang and Wu, 1990); Xiong'er Group (He et al., 2010; Peng et al., 2008; Wang et al., 2010); mantle-derived basaltic magma (B): Sr = 150 ppm, $I_{\text{Sr}} = 0.704$, Nd = 15 ppm, $\varepsilon_{\text{Nd}} = 8$ (Jahn et al., 1999); Cretaceous granite from the southern margin of the NCC values are from Gao et al. (2010), Guo et al. (2009) and Zhao et al. (2012); (b) the Taihua Group metamorphic basement rocks: (Diwu et al., 2010; Liu et al., 2009; Xu et al., 2009a); the Xiong'er Group: (Wang et al., 2010).

Roberts and Clemens, 1993; Sylvester, 1998; Zhao et al., 2013a). Xu et al. (2009b) pointed out that the partial melting of crust can be triggered by thermal transmission between crust and mantle and relay on the underplating of mantle-derived magmas. The upwelling asthenosphere can provide sufficient heat to melt the lithospheric mantle, resulting in voluminous mafic magmas. Underplating of the mafic magmas induced partial melting of the thickened lower crust, and led to formation of voluminous felsic magmas (Wu et al., 2005a; Chen et al., 2008a; Mao et al., 2010; Pei et al., 2011). The identification of the magma mixing in the Funiushan granites reflects a strong mantle–crust interaction in the early Cretaceous in the southern margin of the NCC. The underplated basaltic magmas supplied both energy and materials for the formation of the granites. Increment of the mantle materials in the granites with time indicates the increasing mantle–crust interaction and progressive lithospheric thinning and extensional setting in the region.

A notable feature is the roughly east–west-trending distribution of the granitic plutons (Fig. 1b). The Triassic Luan-Chuan suture zone between the Qinling micro-continent and the NCC (Li et al., 1993; Liu and Zhang, 2008) probably played a major role for the regional alignment of the granites (Wang et al., 2007a; Guo et al., 2009). Therefore, the extensional event was considered to be related to the evolution of the QOB (Chen et al., 2008b; Wang et al., 2008; Guo et al., 2009). Zhang et al. (1996) proposed that continental collision in the QOB took place during the early Mesozoic (245–235 Ma) with an intracontinental subduction in its early

stage. In this period, the lithosphere was strongly compressed, shortened and thickened, leading to the Luonan–Luanchuan over-thrust system on the southern margin of the NCC (Zhang et al., 2001). Geochronological and geochemical data of igneous rocks suggest a post-collisional extensional setting in the late Triassic (Zhang et al., 1999, 2008; Wang et al., 2007b; Qin et al., 2009; Ding et al., 2011), which was almost 100 Mys older than the granites along the southern margin of the NCC. However, the post-collisional magmatism generally lasted within 50 Mys for an orogenic cycle (e.g. Van Staal and De Roo, 1995; Finger et al., 1997; Liégeois et al., 1998; Waught et al., 1998; Bea et al., 1999; Van Wagoner et al., 2002). We therefore suggest that the crustal extension and lithospheric thinning in the southern margin of the NCC were probably controlled by an independent geodynamic setting.

The Jurassic–Cretaceous tectonic reactivation and lithospheric thinning of the eastern NCC coincides in time with a significant increase in the growth rate and a larger change in the subduction direction of the Pacific plate (e.g. Bartolini and Larson, 2001; Sun et al., 2007). Such a temporal coincidence implies that the westward subduction of the Pacific plate may have played critical roles in the destruction of the NCC. Consequently, many researchers attribute Pacific slab subduction from the east as the major cause for lithospheric thinning (Fig. 11) (e.g. Zhao et al., 2007a; Zhao and Ohtani, 2009; Zhu et al., 2010, 2012a; Xu et al., 2011a,b; Li et al., 2012a; Guo et al., 2013; Tang et al., 2013; Goldfarb and Santosh, 2014). Recent seismic topographic imaging has revealed the stagnant subducting Pacific slab in the mantle transition zone

Table 5

LA-MC-ICP-MS zircon Hf isotopic data of the Funiushan pluton.

Spot	$^{176}\text{Yb}/^{177}\text{Hf}$	$^{176}\text{Lu}/^{177}\text{Hf}$	$^{176}\text{Hf}/^{177}\text{Hf}$	$\varepsilon_{\text{Hf}}(t)$	T_{DM1} (Ma)	T_{DM}^{C}	$f_{\text{Lu/Hf}}$
<i>FN-46 (t = 131 Ma)</i>							
FN-46-01	0.013499	0.000608	0.281904	-27.9	1877	2930	-0.98
FN-46-02	0.024122	0.001022	0.282429	-9.4	1165	1777	-0.97
FN-46-03	0.032895	0.001364	0.282356	-12.0	1279	1942	-0.96
FN-46-05	0.030050	0.001279	0.282332	-12.8	1309	1993	-0.96
FN-46-06	0.012940	0.000612	0.282241	-15.9	1412	2190	-0.98
FN-46-07	0.025884	0.001114	0.282394	-10.6	1217	1856	-0.97
FN-46-08	0.009097	0.000474	0.282262	-15.2	1379	2144	-0.99
FN-46-09	0.007398	0.000389	0.282263	-15.2	1374	2141	-0.99
FN-46-10	0.018763	0.000855	0.282211	-17.0	1463	2258	-0.97
FN-46-11	0.006990	0.000357	0.282207	-17.1	1450	2264	-0.99
FN-46-12	0.011780	0.000583	0.282225	-16.5	1434	2226	-0.98
FN-46-13	0.009371	0.000488	0.282191	-17.7	1477	2301	-0.99
FN-46-14	0.010887	0.000565	0.282272	-14.9	1368	2122	-0.98
FN-46-15	0.018618	0.000869	0.282206	-17.2	1471	2270	-0.97
FN-46-16	0.009605	0.000490	0.282392	-10.6	1200	1857	-0.99
FN-46-17	0.011528	0.000541	0.282222	-16.6	1436	2232	-0.98
FN-46-19	0.027252	0.001164	0.282408	-10.1	1199	1825	-0.96
FN-46-20	0.017008	0.000788	0.282242	-16.0	1418	2190	-0.98
FN-46-21	0.033681	0.001329	0.282572	-4.3	971	1459	-0.96
FN-46-23	0.042440	0.001725	0.282408	-10.2	1217	1828	-0.95
<i>FN-63 (t = 115 Ma)</i>							
FN-63-01	0.036406	0.001586	0.282476	-8.1	1116	1686	-0.95
FN-63-02	0.030781	0.001455	0.282520	-6.5	1049	1586	-0.96
FN-63-03	0.031000	0.001332	0.282310	-14.0	1343	2052	-0.96
FN-63-04	0.057237	0.002258	0.282414	-10.3	1226	1825	-0.93
FN-63-05	0.040573	0.001620	0.282437	-9.5	1172	1771	-0.95
FN-63-06	0.080136	0.003122	0.282552	-5.5	1051	1524	-0.91
FN-63-07	0.021221	0.000924	0.282549	-5.5	994	1519	-0.97
FN-63-08	0.044615	0.001816	0.282481	-7.9	1116	1675	-0.95
FN-63-09	0.031781	0.001295	0.282454	-8.8	1138	1732	-0.96
FN-63-10	0.030362	0.001314	0.282428	-9.8	1176	1791	-0.96
FN-63-11	0.016331	0.000732	0.282208	-17.5	1463	2273	-0.98
FN-63-12	0.023900	0.000921	0.282553	-5.3	988	1510	-0.97
FN-63-13	0.020153	0.000893	0.282570	-7.1	963	1501	-0.97
FN-63-14	0.024650	0.001053	0.282473	-8.2	1104	1688	-0.97
FN-63-15	0.038598	0.001817	0.282476	-8.1	1123	1686	-0.95
FN-63-16	0.031796	0.001292	0.282447	-9.1	1149	1749	-0.96
FN-63-17	0.031931	0.001440	0.282518	-6.6	1052	1591	-0.96
FN-63-18	0.035624	0.001516	0.282434	-9.6	1173	1777	-0.95
FN-63-19	0.049396	0.001990	0.282496	-7.4	1100	1643	-0.94
FN-63-20	0.049186	0.002131	0.282454	-8.9	1165	1737	-0.94
FN-63-21	0.033702	0.001378	0.282466	-8.4	1124	1707	-0.96
FN-63-22	0.043133	0.001814	0.282525	-6.4	1052	1577	-0.95
FN-63-23	0.032861	0.001364	0.282476	-8.1	1109	1684	-0.96
FN-63-24	0.038900	0.001640	0.282486	-7.7	1102	1662	-0.95
<i>FN-89 (t = 117 Ma)</i>							
FN-89-01	0.033152	0.001333	0.282503	-7.1	1070	1623	-0.96
FN-89-02	0.026306	0.001097	0.282511	-6.8	1052	1603	-0.97
FN-89-03	0.026205	0.001103	0.282493	-7.4	1078	1644	-0.97
FN-89-04	0.037615	0.001608	0.282469	-8.3	1126	1699	-0.95
FN-89-05	0.032117	0.001301	0.282462	-8.5	1127	1713	-0.96
FN-89-06	0.040524	0.001651	0.282440	-9.3	1169	1763	-0.95
FN-89-07	0.035252	0.001403	0.282472	-8.2	1115	1690	-0.96
FN-89-08	0.026973	0.001115	0.282428	-9.7	1170	1788	-0.97
FN-89-09	0.016214	0.000714	0.282469	-8.2	1099	1694	-0.98
FN-89-10	0.021983	0.000914	0.282465	-8.4	1111	1704	-0.97
FN-89-11	0.033498	0.001328	0.282293	-14.5	1366	2088	-0.96
FN-89-13	0.033582	0.001291	0.282622	-2.9	900	1356	-0.96
FN-89-14	0.025767	0.001076	0.282408	-10.4	1196	1831	-0.97
FN-89-15	0.028054	0.001099	0.282475	-8.1	1102	1683	-0.97
FN-89-17	0.038781	0.001543	0.282527	-6.2	1041	1568	-0.95
FN-89-19	0.037028	0.001476	0.282563	-5.0	989	1489	-0.96
FN-89-20	0.028431	0.001171	0.282467	-8.3	1115	1700	-0.96
FN-89-21	0.036039	0.001450	0.282446	-9.1	1155	1750	-0.96
FN-89-22	0.030853	0.001288	0.282458	-8.7	1133	1722	-0.96
FN-89-23	0.028832	0.001196	0.282467	-7.6	1116	1683	-0.96
FN-89-24	0.031038	0.001278	0.282509	-6.9	1060	1608	-0.96
<i>FN-126 (t = 115 Ma)</i>							
FN-126-01	0.012045	0.000607	0.282460	-8.6	1109	1716	-0.98
FN-126-02	0.041356	0.001752	0.282730	0.9	756	1118	-0.95
FN-126-04	0.029248	0.001211	0.282518	-6.6	1045	1589	-0.96
FN-126-05	0.030887	0.001375	0.282501	-7.2	1074	1628	-0.96

(continued on next page)

Table 5 (continued)

Spot	$^{176}\text{Yb}/^{177}\text{Hf}$	$^{176}\text{Lu}/^{177}\text{Hf}$	$^{176}\text{Hf}/^{177}\text{Hf}$	$\varepsilon_{\text{Hf}}(t)$	T_{DM1} (Ma)	T_{DM}^{C}	$f_{\text{Lu/Hf}}$
FN-126-06	0.029352	0.001298	0.282463	-8.5	1125	1712	-0.96
FN-126-07	0.004973	0.000313	0.282508	-6.8	1035	1607	-0.99
FN-126-08	0.038781	0.001555	0.282501	-7.2	1079	1629	-0.95
FN-126-09	0.065003	0.002635	0.282573	-4.7	1006	1474	-0.92
FN-126-10	0.022368	0.001000	0.282545	-5.6	1001	1527	-0.97
FN-126-11	0.033505	0.001525	0.282462	-8.6	1134	1716	-0.95
FN-126-12	0.023185	0.001053	0.282470	-8.3	1109	1696	-0.97
FN-126-13	0.016139	0.000751	0.282473	-8.1	1095	1687	-0.98
FN-126-14	0.040385	0.001633	0.282487	-7.7	1101	1659	-0.95
FN-126-15	0.035167	0.001500	0.282520	-6.5	1051	1587	-0.95
FN-126-16	0.036620	0.001511	0.282456	-8.8	1142	1728	-0.95
FN-126-17	0.037521	0.001536	0.282487	-7.7	1099	1660	-0.95
FN-126-18	0.021605	0.000922	0.282386	-11.2	1222	1882	-0.97
FN-126-19	0.031322	0.001303	0.282508	-6.9	1062	1612	-0.96
FN-126-20	0.049686	0.002033	0.282542	-5.8	1034	1540	-0.94
FN-126-21	0.017237	0.000826	0.282464	-8.4	1110	1708	-0.98
FN-126-22	0.022795	0.001032	0.282467	-8.4	1112	1702	-0.97
FN-126-23	0.028747	0.001181	0.282436	-9.5	1161	1773	-0.96
FN-126-24	0.030165	0.001230	0.282436	-9.5	1162	1773	-0.96

The notations of $\varepsilon_{\text{Hf}}(t)$, $f_{\text{Lu/Hf}}$ and T_{Hf} are defined as $\varepsilon_{\text{Hf}}(t) = ((^{176}\text{Hf}/^{177}\text{Hf})_{\text{S}}/(^{176}\text{Hf}/^{177}\text{Hf})_{\text{CHUR,0}} - 1) \times 10,000$; $\varepsilon_{\text{Hf}}(t) = ((^{176}\text{Hf}/^{177}\text{Hf})_{\text{S}} - (^{176}\text{Lu}/^{177}\text{Hf})_{\text{S}} \times (e^{xt} - 1)) / ((^{176}\text{Hf}/^{177}\text{Hf})_{\text{S}} - (^{176}\text{Lu}/^{177}\text{Hf})_{\text{DM}})$; $f_{\text{Lu/Hf}} = (^{176}\text{Lu}/^{177}\text{Hf})_{\text{S}} / (^{176}\text{Lu}/^{177}\text{Hf})_{\text{CHUR}} - 1$. ($^{176}\text{Lu}/^{177}\text{Hf}$)_S and ($^{176}\text{Hf}/^{177}\text{Hf}$)_S are the measured values of samples, ($^{176}\text{Lu}/^{177}\text{Hf}$)_{CHUR} = 0.03321 and ($^{176}\text{Hf}/^{177}\text{Hf}$)_{CHUR,0} = 0.282772 (Blichert-Toft and Albarède, 1997); ($^{176}\text{Lu}/^{177}\text{Hf}$)_{DM} = 0.03842 and ($^{176}\text{Hf}/^{177}\text{Hf}$)_{DM} = 0.28325 (Griffin et al., 2000), t = crystallization time of zircon. $\lambda = 1.867 \times 10^{-11} \text{ year}^{-1}$ (Soderlund et al., 2004), $f_{\text{Lu/Hf}} = -0.55$ (Vervoort et al., 1996) was used in our calculations.

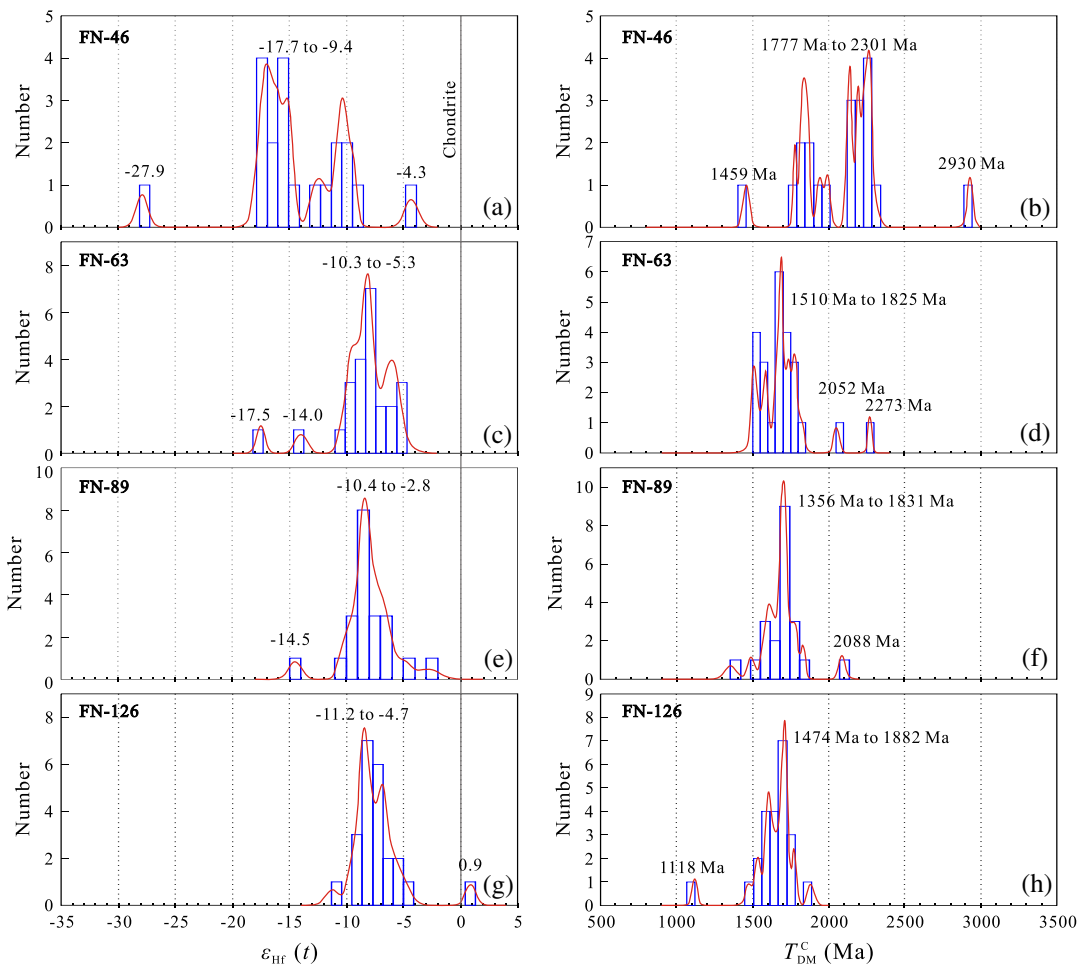


Fig. 8. Histograms of $\varepsilon_{\text{Hf}}(t)$ values and T_{DM}^{C} ages of zircons in the Funiushan pluton.

beneath the eastern NCC, with the western edge of the slab overlapping the North–South Gravity Lineament that separates the tectonically reactivated Eastern Block from the relatively stable

Western Block of the NCC (Fig. 11; Huang and Zhao, 2006; Xu et al., 2011a,b; Guo et al., 2013). The subduction of the Paleo-Pacific plate may have exerted a stronger influence on the east than

Table 6

Partition coefficients and presumed source for trace element modeling.

Element	Taihua Group	Partition coefficients				Melt fraction			
		Amphibolite (ppm)	Am	Cpx	Pl	Bulk D (70:10:20)*	5% (ppm)	10% (ppm)	20% (ppm)
Rb	42.2		0.06	0.02	0.105	0.07	377	266	167
Ba	542		0.17	0.08	0.16	0.16	2698	2231	1658
Th	3.01		0.03	0.04	0.1	0.05	32.5	21.4	12.8
U	0.65		0.06	0.04	0.093	0.06	5.79	4.08	2.56
Nb	7.89		0.31	0.0029	0.025	0.22	30.2	26.3	20.9
Ta	0.42		0.26	0.08	0.035	0.20	1.75	1.50	1.16
K	12,309		0.31	0.09	0.1	0.25	43,386	38,297	31,020
La	16.1		0.2	0.075	0.302	0.21	64.9	56.0	43.9
Ce	37.3		0.42	0.131	0.221	0.35	97.2	89.6	77.6
Sr	270		0.36	0.073	1.8	0.62	423	411	388
Nd	23.8		1.14	0.379	0.149	0.87	27.3	27.1	26.6
Zr	147		0.5	0.24	0.013	0.38	361	335	294
Hf	3.65		0.69	0.37	0.015	0.52	6.68	6.40	5.91
Sm	5.54		1	0.59	0.102	0.78	7.01	6.92	6.73
Eu	1.68		1.62	0.69	1.214	1.21	1.18	1.20	1.24
Ti	0.56		2.77	0.7	0.05	2.02	0.28	0.29	0.31
Gd	5.57		1.9	0.84	0.067	1.43	3.96	4.02	4.15
Tb	0.95		2.96	0.67		2.14	0.46	0.47	0.50
Dy	5.41		1.88	1.05	0.05	1.43	3.83	3.89	4.02
Y	33.0		2.1	1.63	0.06	1.65	20.5	20.9	21.8
Ho	1.17		2.3	1.67		1.78	0.68	0.69	0.72
Er	3.29		2.01	1.19	0.045	1.54	2.18	2.22	2.30
Yb	3.07		2.33	0.86	0.041	1.73	1.82	1.86	1.94
Lu	0.46		2.1	0.92	0.039	1.57	0.30	0.31	0.32

The amphibolite of the Taihua Group estimate of Zhou et al. (1997), Lin (2006) and Huang et al. (2010) has been taken as presumed source. Selected partition coefficients are from felsic magmas; and from experimental runs under equilibrium conditions similar to normal granite if possible. For example, Partition coefficients of trace element for amphibole are from an experimental run at 925 °C, 1.0 Gpa (Xiong, 2006). Data sources for partition coefficients are: Ds. for amphibole, from Xiong (2006) and Klein et al. (1997); for clinopyroxene, from Klein et al. (2000) and Barth et al. (2002); for plagioclase, from Rollinson (1993). Representative calculations are listed for batch melting with residue as 70% amphibole + 10% clinopyroxene + 20% plagioclase(*)).

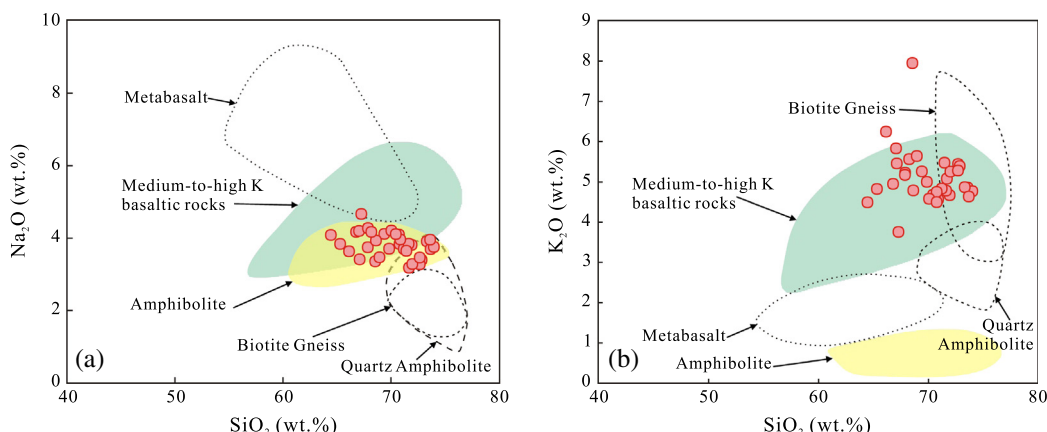


Fig. 9. The (a) Na₂O and (b) K₂O composition of the rocks from the Funiushan pluton with published data for experimental melts. Experimentally produced glasses are from Beard and Lofgren (1991) (amphibolites; 1, 3, 6, 9 kb; 800–1000 °C), Rapp and Watson (1995) (metabasalt; 8–32 kb; 1000–1125 °C), Douce and Beard (1995) (quartz amphibolites; 3–15 kb; 850–930 °C; biotite gneiss; 3–15 kb; 850–930 °C) and Sisson et al. (2005) (medium to high K basaltic rocks; 700 Mpa; 825–975 °C).

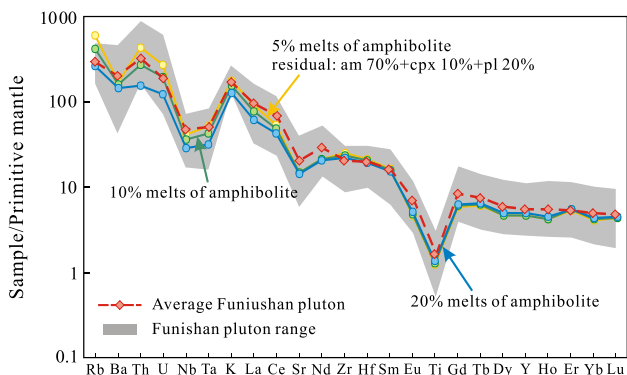


Fig. 10. Trace element modeling of partial melting of Taihua Group basement rocks. Parameters are from Table 6. am-amphibole, cpx-clinopyroxene, pl-plagioclase.

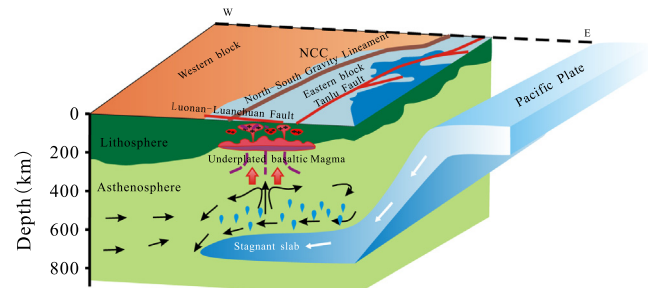


Fig. 11. The geodynamic control on the thinning/destruction of the eastern NCC and the resultant magmatism (modified from Li et al., 2012a). See text for explanation. NCC = North China Craton.

the west part of the NCC, explaining the phenomenon that widespread late Mesozoic granitic intrusions in the eastern QOB but not in the western QOB (Fig. 11). The asthenosphere upwelling and lithospheric thinning may occur mainly along major rupture zones that penetrate the lithospheric mantle along the margins of the NCC (Zhu et al., 2010). This can explain the linear distribution of granitic intrusions along crustal-scale structures such as the Luonan – Luanchuan Faults (Fig. 1B).

6. Conclusions

- (1) The Funiushan I-type granites in the southern margin of the North China Craton formed at 131–115 Ma.
- (2) The rocks were dominantly produced by partial melting of amphibolites of the Taihua Group, with mixed with the mantle-derived basaltic magma.
- (3) The granites record evidence for a strong crust–mantle interaction, and formed in an intracontinental extensional setting which was related to lithospheric thinning and asthenospheric upwelling in this region, which was possibly caused by westward subduction of the Paleo-Pacific plate, not post-orogenic collapse process of the QOB.

Acknowledgements

This study was funded by the National Natural Science Foundation of China (No. 41373046). We thank Prof. Meifu Zhou, Prof. Junhong Zhao, Prof. Qing Qian and Dr. Alexandra Yang Yang for helpful comments on an early version of the manuscript. We appreciate the assistance of Dr. Yanyan Zhou for zircon age analyses and Dr. Alexandra Yang Yang for trace elements analyses. We also sincerely thank Dr. Fenlian Wang and Mr. Xinhao Li for their capable field assistant. We are grateful to two anonymous reviewers and editor in-chief Dr. Bor-ming Jahn and associate editor Dr. M. Santosh for careful and constructive comments and editorial handling which significantly improved the manuscript. This is contribution No. IS-1945 from GIGCAS.

Appendix A. Supplementary material

Supplementary data associated with this article can be found, in the online version, at <http://dx.doi.org/10.1016/j.jseas.2014.07.042>.

References

- Bao, Z.W., Wang, C.Y., Zhao, T.P., Li, C.J., Gao, X.Y., 2014. Petrogenesis of the Mesozoic granites and Mo mineralization of the Luanchuan ore field in the East Qinling Mo mineralization belt, Central China. *Ore Geol. Rev.* 57, 132–153.
- Barth, M.G., Foley, S.F., Horn, I., 2002. Partial melting in Archean subduction zones: constraints from experimentally determined trace element partition coefficients between eclogitic minerals and tonalitic melts under upper mantle conditions. *Precambr. Res.* 113, 323–340.
- Bartolini, A., Larson, R.L., 2001. Pacific microplate and the Pangea supercontinent in the Early to Middle Jurassic. *Geology* 29, 735–738.
- Bea, F., Montero, P., Molina, J.F., 1999. Mafic precursors, peraluminous granitoids, and late lamprophyres in the Avila batholith: a model for the generation of Variscan batholiths in Iberia. *J. Geol.* 107, 399–419.
- Beard, J., Lofgren, G., 1991. Partial melting of basaltic and andesitic greenstones and amphibolites under dehydration melting and water-saturated conditions at 1, 3, and 6.9 kilobars. *J. Petrol.* 32, 365–401.
- Belousova, E., Griffin, W.L., O'Reilly, S.Y., Fisher, N., 2002. Igneous zircon: trace element composition as an indicator of source rock type. *Contrib. Miner. Petrol.* 143, 602–622.
- Bird, P., 1978. Initiation of intracontinental subduction in the Himalaya. *J. Geophys. Res.: Solid Earth* 83, 4975–4987.
- Blichert-Toft, J., Albarède, F., 1997. The Lu-Hf isotope geochemistry of chondrites and the evolution of the mantle–crust system. *Earth Planet. Sci. Lett.* 148, 243–258.
- Chappell, B., 1999. Aluminium saturation in I- and S-type granites and the characterization of fractionated haplogranites. *Lithos* 46, 535–551.
- Chappell, B., White, A., 1992. I- and S-type granites in the Lachlan Fold Belt. *Trans. Roy. Soc. Edinburgh: Earth Sci.* 83, 1–26.
- Chen, Y.J., Li, C., Zhang, J., Li, Z., Wang, H.H., 2000. Sr and O isotopic characteristics of porphyries in the Qinling molybdenum deposit belt and their implication to genetic mechanism and type. *Sci. China, Ser. D Earth Sci.* 43, 82–94.
- Chen, B., Tian, W., Jahn, B.M., Chen, Z.C., 2008a. Zircon SHRIMP U-Pb ages and in-situ Hf isotopic analysis for the Mesozoic intrusions in South Taihang, North China craton: evidence for hybridization between mantle-derived magmas and crustal components. *Lithos* 102, 118–137.
- Chen, Y.J., Pirajno, F., Qi, J.P., 2008b. The Shanggong gold deposit, Eastern Qinling Orogen, China: isotope geochemistry and implications for ore genesis. *J. Asian Earth Sci.* 33, 252–266.
- Chen, Y.J., Pirajno, F., Li, N., Guo, D.S., Lai, Y., 2009. Isotope systematics and fluid inclusion studies of the Qiyugou breccia pipe-hosted gold deposit, Qinling Orogen, Henan province, China: implications for ore genesis. *Ore Geol. Rev.* 35, 245–261.
- Ding, L.X., Ma, C.Q., Li, J.W., Robinson, P.T., Deng, X.D., Zhang, C., Xu, W.C., 2011. Timing and genesis of the adakitic and shoshonitic intrusions in the Laoniushan complex, southern margin of the North China Craton: implications for post-collisional magmatism associated with the Qinling Orogen. *Lithos* 126, 212–232.
- Diwu, C.R., Sun, Y., Lin, C.L., Wang, H.L., 2010. LA-(MC)-ICPMS U-Pb zircon geochronology and Lu-Hf isotope compositions of the Taihua complex on the southern margin of the North China Craton. *Chin. Sci. Bull.* 55, 2557–2571.
- Dong, Y., Zhang, G., Neubauer, F., Liu, X., Genser, J., Hauzenberger, C., 2011. Tectonic evolution of the Qinling orogen, China: review and synthesis. *J. Asian Earth Sci.* 41 (3), 213–237.
- Douce, A.E.P., Beard, J.S., 1995. Dehydration-melting of biotite gneiss and quartz amphibolite from 3 to 15 kbar. *J. Petrol.* 36, 707–738.
- Finger, F., Roberts, M., Haunschmid, B., Schermaier, A., Steyrer, H., 1997. Variscan granitoids of central Europe: their typology, potential sources and tectono-thermal relations. *Mineral. Petrol.* 61, 67–96.
- Gao, S., Rudnick, R.L., Yuan, H.L., Liu, X.M., Liu, Y.S., Xu, W.L., Ling, W.L., Ayers, J., Wang, X.C., Wang, Q.H., 2004. Recycling lower continental crust in the North China craton. *Nature* 432, 892–897.
- Gao, X.Y., Zhao, T.P., Yuan, Z.L., Zhou, Y.Y., Gao, J.F., 2010. Geochemistry and petrogenesis of the Heyu batholith in the southern margin of the North China block. *Acta Petrol. Sin.* 26, 3485–3506 (in Chinese with English abstract).
- Goldfarb, R.J., Santosh, M., 2014. The dilemma of the Jiaodong gold deposits: are they unique? *Geosci. Front.* 5, 139–153.
- Griffin, W.L., Pearson, N.J., Belousova, E., Jackson, S.E., Achterbergh, E.V., O'Reilly, S.Y., Shee, S.R., 2000. The Hf isotope composition of cratonic mantle: LAM-MC-ICPMS analysis of zircon megacrysts in kimberlites. *Geochim. Cosmochim. Acta* 64 (1), 133–147.
- Guo, B., Zhu, L.M., Li, B., Gong, H.J., Wang, J.Q., 2009. Zircon U-Pb age and Hf isotope composition of the Huashan and Heyu granite plutons at the southern margin of North China Craton: implications for geodynamic setting. *Acta Petrol. Sin.* 25, 265–281 (in Chinese with English abstract).
- Guo, P., Santosh, M., Li, S., 2013. Geodynamics of gold metallogeny in the Shandong Province, NE China: an integrated geological, geophysical and geochemical perspective. *Gondwana Res.* 24 (3), 1172–1202.
- He, Y.H., Zhao, G.C., Sun, M., Han, Y.G., 2010. Petrogenesis and tectonic setting of volcanic rocks in the Xiaoshan and Waifangshan areas along the southern margin of the North China Craton: constraints from bulk-rock geochemistry and Sr-Nd isotopic composition. *Lithos* 114, 186–199.
- HIGS (Henan Institute of Geological Survey), 2002. Report of Regional Geological Survey of Neixiang, Henan province, China, pp. 201–204.
- Hu, Z.H., Hu, S.X., Zhou, S.Z., 1990. The Yanshanian A-type twin granite belts of intracontinental compression–subduction environment in northern part of east Qinling area. *Acta Petrol. Sin.* 6 (1), 1–12 (in Chinese with English abstract).
- Hu, J., Jiang, S.Y., Zhao, H.X., Shao, Y., Zhang, Z.Z., Xiao, E., Wang, Y.F., Dai, B.Z., Li, H.Y., 2012. Geochemistry and petrogenesis of the Huashan granites and their implications for the Mesozoic tectonic settings in the Xiaoqinling gold mineralization belt, NW China. *J. Asian Earth Sci.* 56, 276–289.
- Huang, X., Wu, L.R., 1990. Nd-Sr isotopes of granitoids from Shanxi Province and their significance for tectonic evolution. *Acta Petrol. Sin.* 6, 1–11 (in Chinese).
- Huang, J.L., Zhao, D.P., 2006. High-resolution mantle tomography of China and surrounding regions. *J. Geophys. Res.* 111, 1–21.
- Huang, X.L., Niu, Y., Xu, Y.G., Yang, Q.J., Zhong, J.W., 2010. Geochemistry of TTG and TTG-like gneisses from Lushan-Taihua complex in the southern North China Craton: implications for late Archean crustal accretion. *Precambr. Res.* 182, 43–56.
- Jahn, B.M., Wu, F.Y., Lo, C.H., Tsai, C.H., 1999. Crust–mantle interaction induced by deep subduction of the continental crust: geochemical and Sr-Nd isotopic evidence from post-collisional mafic-ultramafic intrusions of the northern Dabie complex, central China. *Chem. Geol.* 157, 119–146.
- Kemp, A., Wormald, R., Whitehouse, M., Price, R., 2005. Hf isotopes in zircon reveal contrasting sources and crystallization histories for alkaline to peralkaline granites of Temora, southeastern Australia. *Geology* 33, 797–800.
- King, P., White, A., Chappell, B., Allen, C., 1997. Characterization and origin of aluminous A-type granites from the Lachlan Fold Belt, southeastern Australia. *J. Petrol.* 38, 371–391.
- King, P., Chappell, B., Allen, C., White, A., 2001. Are A-type granites the high-temperature felsic granites? Evidence from fractionated granites of the Wangrah Suite. *Aust. J. Earth Sci.* 48, 501–514.

- Klein, M., Stosch, H.G., Seck, H., 1997. Partitioning of high field-strength and rare-earth elements between amphibole and quartz-dioritic to tonalitic melts: an experimental study. *Chem. Geol.* 138, 257–271.
- Klein, M., Stosch, H.G., Seck, H., Shimizu, N., 2000. Experimental partitioning of high field strength and rare earth elements between clinopyroxene and garnet in andesitic to tonalitic systems. *Geochim. Cosmochim. Acta* 64, 99–115.
- Kröner, A., Compston, W., Zhang, G.W., Guo, A.L., Todt, W., 1988. Age and tectonic setting of Late Archean greenstone-gneiss terrain in Henan Province, China, as revealed by single-grain zircon dating. *Geology* 16, 211–215.
- Li, S.R., Santosh, M., 2014. Metallogeny and craton destruction: records from the North China Craton. *Ore Geol. Rev.* 56, 376–414.
- Li, S.G., Xiao, Y.L., Liou, D.L., Chen, Y.Z., Ge, N.J., Zhang, Z.Q., Sun, S.S., Cong, B.L., Zhang, R.Y., Hart, S.R., Wang, S.S., 1993. Collision of the North China and Yangtze Blocks and formation of coesite-bearing eclogites: timing and processes. *Chem. Geol.* 109, 89–111.
- Li, X.H., Liu, D.Y., Sun, M., Li, W.X., Liang, X.R., Liu, Y., 2004. Precise Sm–Nd and U–Pb isotopic dating of the supergiant Shizhuoyuan polymetallic deposit and its host granite, SE China. *Geol. Mag.* 141, 225–231.
- Li, J.W., Bi, S.J., Selby, D., Chen, L., Vasconcelos, P., Thiede, D., Zhou, M.F., Zhao, X.F., Li, Z.K., Qiu, H.N., 2012a. Giant Mesozoic gold provinces related to the destruction of the North China craton. *Earth Planet. Sci. Lett.* 349, 26–37.
- Li, N., Chen, Y.J., Pirajno, F., Gong, H.J., Mao, S.D., Ni, Z.Y., 2012b. LA-ICP-MS zircon U–Pb dating, trace element and Hf isotope geochemistry of the Heyu granite batholith, eastern Qinling, central China: Implications for Mesozoic tectono-magmatic evolution. *Lithos* 142–143, 34–47.
- Li, N., Chen, Y.J., Santosh, M., Pirajno, F., 2013. Compositional polarity of Triassic granitoids in the Qinling Orogen, China: implication for termination of the northernmost paleo-Tethys. *Gondwana Res.*. <http://dx.doi.org/10.1016/j.gr.2013.09.017>.
- Li, S.R., Santosh, M., Zhang, H.F., Shen, J.F., Dong, G.C., Wang, J.Z., Zhang, J.Q., 2013. Inhomogeneous lithospheric thinning in the central North China Craton: zircon U–Pb and S–He–Ar isotopic record from magmatism and metallogeny in the Taihang Mountains. *Gondwana Res.* 23 (1), 141–160.
- Liégeois, J.P., Navez, J., Hertogen, J., Black, R., 1998. Contrasting origin of post-collisional high-K calc-alkaline and shoshonitic versus alkaline and peralkaline granitoids. The use of sliding normalization. *Lithos* 45, 1–28.
- Lin, C.L., 2006. Geochemistry, Geochronology and Tectonic Settings of Archean Gneisses in Lushan, Henan Province. Master Degree Thesis. Xi'an: Northwestern University, pp. 1–89 (in Chinese with English abstract).
- Liu, S.F., Zhang, G.W., 2008. Evolution and geodynamics of basin/mountain systems in east Qinling-Dabieshan and its adjacent regions, China. *Geol. Bull. China* 27, 1943–1960.
- Liu, D.Y., Wilde, S.A., Wan, Y.S., Wang, S.Y., Valley, J.W., Kita, N., Dong, C.Y., Xie, H.Q., Yang, C.X., Zhang, Y.X., Gao, L.Z., 2009. Combined U–Pb, hafnium and oxygen isotope analysis of zircons from meta-igneous rocks in the southern North China Craton reveal multiple events in the Late Mesoarchean-Early Neoarchean. *Chem. Geol.* 261, 140–154.
- Lu, S.W., 1995. Geological characteristics of granite in Funiushan region and its genesis. *Henan Geol.* 13, 183–190 (in Chinese with English abstract).
- Mao, J.W., Xie, G.Q., Bierlein, F., Qiu, W.J., Du, A.D., Ye, H.S., Pirajno, F., Li, H.M., Guo, B.J., Li, Y.F., Yang, Z.Q., 2008. Tectonic implications from Re–Os dating of Mesozoic molybdenum deposits in the East Qinling-Dabie orogenic belt. *Geochim. Cosmochim. Acta* 72, 4607–4626.
- Mao, J.W., Xie, G.Q., Pirajno, F., Ye, H.S., Wang, Y.B., Li, Y.F., Xiang, J.F., Zhao, H.J., 2010. Late Jurassic-Early Cretaceous granitoid magmatism in Eastern Qinling, central-eastern China: SHRIMP zircon U–Pb ages and tectonic implications. *Aust. J. Earth Sci.* 57, 51–78.
- Martin, H., Smithies, R., Rapp, R., Moyen, J.F., Champion, D., 2005. An overview of adakite, tonalite-trondhjemite-granodiorite (TTG), and sanukitoid: relationships and some implications for crustal evolution. *Lithos* 79, 1–24.
- Ni, Z.Y., Chen, Y.J., Li, N., Zhang, H., 2012. Pb–Sr–Nd isotope constraints on the fluid source of the Dahu Au–Mo deposit in Qinling Orogen, central China, and implication for Triassic tectonic setting. *Ore Geol. Rev.* 46, 60–67.
- Pei, F.P., Xu, W.L., Yang, D.B., Yu, Y., Wang, W., Zhao, Q.G., 2011. Geochronology and geochemistry of Mesozoic mafic-ultramafic complexes in the southern Liaoning and southern Jilin provinces, NE China: constraints on the spatial extent of destruction of the North China Craton. *J. Asian Earth Sci.* 40, 636–650.
- Peng, P., Zhai, M.G., Ernst, R.E., Guo, J.H., Liu, F.L., Hu, B., 2008. A 1.78 Ga large igneous province in the North China craton: the Xiong'er Volcanic Province and the North China dyke swarm. *Lithos* 101, 260–280.
- Pertermann, M., Hirschmann, M.M., Hametner, K., Günther, D., Schmidt, M.W., 2004. Experimental determination of trace element partitioning between garnet and silica-rich liquid during anhydrous partial melting of MORB-like eclogite. *Geochem. Geophys. Geosyst.* 5. <http://dx.doi.org/10.1029/2003GC000638>.
- Qin, J.F., Lai, S.C., Grapes, R., Diwu, C.R., Ju, Y.J., Li, Y.F., 2009. Geochemical evidence for origin of magma mixing for the Triassic monzonitic granite and its enclaves at Mishuling in the Qinling orogen (central China). *Lithos* 112, 259–276.
- Rapp, R.P., Watson, E.B., 1995. Dehydration melting of metabasalt at 8–32 kbar: implications for continental growth and crust–mantle recycling. *J. Petrol.* 36, 891–931.
- Ratschbacher, L., Hacker, B.R., Calvert, A., Webb, L.E., Grimmer, J.C., McWilliams, M.O., Ireland, T., Dong, S., Hu, J., 2003. Tectonics of the Qinling (Central China): tectonostratigraphy, geochronology, and deformation history. *Tectonophysics* 366, 1–53.
- Roberts, M.P., Clemens, J.D., 1993. Origin of high-potassium, talc-alkaline, I-type granitoids. *Geology* 21, 825–828.
- Rollinson, H.R., 1993. Using Geochemical Data: Evaluation, Presentation, Interpretation. Longman Scientific & Technical Essex, pp. 108–111.
- Rudnick, R., Gao, S., 2003. Composition of the continental crust. *Treatise Geochem.* 3, 1–64.
- Sisson, T., Ratajeski, K., Hankins, W., Glazner, A., 2005. Voluminous granitic magmas from common basaltic sources. *Contrib. Miner. Petro.* 148, 635–661.
- Soderlund, U., Patchett, P.J., Vervoort, J.D., Lachlan, C.E., 2004. The 176Lu decay constant determined by Lu–Hf and U–Pb isotope systematics of Precambrian mafic intrusions. *Earth Planet. Sci. Lett.* 219 (3–4), 311–324.
- Sun, S.S., McDonough, W.F., 1989. Chemical and isotopic systematics of oceanic basalts: implications for mantle composition and processes. *Geol. Soc., London, Spec. Publ.* 42, 313–345.
- Sun, W.D., Ding, X., Hu, Y.H., Li, X.H., 2007. The golden transformation of the Cretaceous plate subduction in the west Pacific. *Earth Planet. Sci. Lett.* 262, 533–542.
- Sylvester, P.J., 1998. Post-collisional strongly peraluminous granites. *Lithos* 45, 29–44.
- Tang, Y.J., Zhang, H.F., Santosh, M., Ying, J.F., 2013. Differential destruction of the North China Craton: a tectonic perspective. *J. Asian Earth Sci.* 78, 71–82.
- Van Staal, C., De Roe, J., 1995. Mid-Paleozoic tectonic evolution of the Appalachian Central Mobile Belt in northern New Brunswick, Canada: collision, extensional collapse and dextral transpression. In: Hibbard, J.P., van Staal, C.R., Cawood, P.A. (Eds.), Current perspectives in the Appalachian-Caledonian Orogen. Geological Association of Canada, Special Paper 41, pp. 367–389.
- Van Wagoner, N.A., Leybourne, M.I., Dadd, K.A., Baldwin, D.K., McNeil, W., 2002. Late Silurian bimodal volcanism of southwestern New Brunswick, Canada: products of continental extension. *Geol. Soc. Am. Bull.* 114, 400–418.
- Vervoort, J.D., Patchett, P.J., Gehrels, G.E., Nutman, A.P., 1996. Constraints on early Earth differentiation from hafnium and neodymium isotopes. *Geochim. Cosmochim. Acta* 60, 3717–3733.
- Waught, T.E., Weaver, S.D., Muir, R.J., 1998. Mid-Cretaceous granitic magmatism during the transition from subduction to extension in southern New Zealand: a chemical and tectonic synthesis. *Lithos* 45, 469–482.
- Wan, Y.S., Wilde, S.A., Liu, D.Y., Yang, C.X., Song, B., Yin, X.Y., 2006. Further evidence for 1.85 Ga metamorphism in the Central Zone of the North China Craton: SHRIMP U–Pb dating of zircon from metamorphic rocks in the Lushan area, Henan Province. *Gondwana Res.* 9, 189–197.
- Wang, J.G., Lu, X.X., 1998. Petrology of the Funiushan granite. *Henan Geol.* 6, 35–40 (in Chinese).
- Wang, F., Lu, X.X., Lo, C.H., Wu, F.Y., He, H.Y., Yang, L.K., Zhu, R.X., 2007a. Post-collisional, potassio monzonite-minette complex (Shahewan) in the Qinling Mountains (central China): 40Ar/39Ar thermochronology, petrogenesis, and implications for the dynamic setting of the Qinling orogen. *J. Asian Earth Sci.* 31, 153–166.
- Wang, X.X., Wang, T., Jahn, B.M., Hu, N.G., Chen, W., 2007b. Tectonic significance of Late Triassic post-collisional lamprophyre dykes from the Qinling Mountains (China). *Geol. Mag.* 144, 837–848.
- Wang, T.H., Mao, J.W., Wang, Y.B., 2008. Research on SHRIMP U–Pb chronology in Xiaoqinling–Xiong’ershan area: the evidence of delamination of lithosphere in Qinling orogenic belt. *Acta Petrol. Sin.* 24, 1273–1287 (in Chinese with English abstract).
- Wang, X.L., Jiang, S.Y., Dai, B.Z., 2010. Melting of enriched Archean subcontinental lithospheric mantle: Evidence from the ca. 1760 Ma volcanic rocks of the Xiong’er Group, southern margin of the North China Craton. *Precambr. Res.* 182, 204–216.
- Watson, E.B., Harrison, T.M., 1983. Zircon saturation revisited: temperature and composition effects in a variety of crustal magma types. *Earth Planet. Sci. Lett.* 64, 295–304.
- Whalen, J.B., Currie, K.L., Chappell, B.W., 1987. A-type granites: geochemical characteristics, discrimination and petrogenesis. *Contrib. Miner. Petro.* 95, 407–419.
- Wilson, M., 1989. Igneous Petrogenesis: A Global Tectonic Approach. Chapman & Hall, London, pp. 13–34.
- Wolf, M.B., London, D., 1994. Apatite dissolution into peraluminous haplogranitic melts: an experimental study of solubilities and mechanisms. *Geochim. Cosmochim. Acta* 58 (19), 4127–4145.
- Wu, Y.B., Zheng, Y.F., 2013. Tectonic evolution of a composite collision orogen: an overview on the Qinling–Tongbai–Hong’an–Dabie–Sulu orogenic belt in central China. *Gondwana Res.* 23, 1402–1428.
- Wu, F.Y., Lin, J.Q., Wilde, S.A., Zhang, X.O., Yang, J.H., 2005a. Nature and significance of the Early Cretaceous giant igneous event in eastern China. *Earth Planet. Sci. Lett.* 233, 103–119.
- Wu, F.Y., Xu, Y.G., Gao, S., Zheng, J.P., 2008. Lithospheric thinning and destruction of the North China Craton. *Acta Petrol. Sin.* 24, 1145–1174 (in Chinese with English abstract).
- Xie, Z., Zheng, Y.F., Zhao, Z.F., Wu, Y.B., Wang, Z.R., Chen, J.F., Liu, X.M., Wu, F.Y., 2006. Mineral isotope evidence for the contemporaneous process of Mesozoic granite emplacement and gneiss metamorphism in the Dabie orogen. *Chem. Geol.* 231, 214–235.
- Xiong, X.L., 2006. Trace element evidence for growth of early continental crust by melting of rutile-bearing hydrous eclogite. *Geology* 34, 945–948.
- Xu, Y.G., 2001. Thermo-tectonic destruction of the Archean lithospheric keel beneath the Sino-Korean Craton in China: evidence, timing and mechanism. *Phys. Chem. Earth Part A* 26, 747–757.
- Xu, Y.G., Huang, X.L., Ma, J.L., Wang, Y.B., Iizuka, Y., Xu, J.F., Wang, Q., Wu, X.Y., 2004. Crust–mantle interaction during the tectono-thermal reactivation of the North

- China Craton: constraints from SHRIMP zircon U-Pb chronology and geochemistry of Mesozoic plutons from western Shandong. *Contrib. Miner. Petrol.* 147, 750–767.
- Xu, X.S., Griffin, W.L., Ma, X., O'Reilly, S.Y., He, Z.Y., Zhang, C.L., 2009a. The Taihua group on the southern margin of the North China craton: further insights from U-Pb ages and Hf isotope compositions of zircons. *Mineral. Petrol.* 97, 43–59.
- Xu, Y.G., Li, H., Pang, C.J., He, B., 2009b. On the timing and duration of the destruction of the North China Craton. *Chin. Sci. Bull.* 54, 3379–3396.
- Xu, W.W., Zheng, T.Y., Zhao, L., 2011a. Mantle dynamics of the reactivating North China Craton: Constraints from the topographies of the 410-km and 660-km discontinuities. *Sci. China Earth Sci.* 54, 881–887.
- Xu, W.W., Zheng, T.Y., Zhao, L., 2011b. Mantle dynamics of the reactivating North China Craton: constraints from the topographies of the 410-km and 660-km discontinuities. *Sci. China – Earth Sci.* 54, 881–887.
- Yang, J.H., Wu, F.Y., Wilde, S.A., Belousova, E., Griffin, W.L., 2008. Mesozoic decratonization of the North China block. *Geology* 36, 467–470.
- Yang, Q.Y., Santosh, M., Shen, J.F., Li, S.R., 2014. Juvenile vs. recycled crust in NE China: Zircon U-Pb geochronology, Hf isotope and an integrated model for Mesozoic gold mineralization in the Jiaodong Peninsula. *Gondwana Res.* 25, 1445–1468.
- Zhai, M., Santosh, M., 2013. Metallogeny of the North China Craton: link with secular changes in the evolving Earth. *Gondwana Res.* 24 (1), 275–297.
- Zhang, H.F., 2012. Destruction of ancient lower crust through magma underplating beneath Jiaodong Peninsula, North China Craton: U-Pb and Hf isotopic evidence from granulite xenoliths. *Gondwana Res.* 21 (1), 281–292.
- Zhang, Z.Q., Li, S.M., 1998. Sm–Nd and Rb–Sr ages of the Archean Taihua Group metamorphic rocks in the Xiong'ershan region, Western Henan province. In: Cheng, Y.Q. (Ed.), Precambrian Geological Research Papers of the North China Platform. Geological Publishing House, Beijing, pp. 123–132.
- Zhang, Z.W., Lu, X.X., 1990. Geochemical characteristics of migmatitic and granitization-type granitoids in Funiushan, Henan, China. *Geochimica* 4, 358–364 (in Chinese with English abstract).
- Zhang, Z.Q., Liu, D.Y., Fu, G.M., 1994. Study on the Isotopic Chronology of Metamorphic Strata in North Qinling. Geological Publishing House, Beijing, pp. 1–143 (in Chinese).
- Zhang, G.W., Guo, A.L., Liu, F.T., Xiao, Q.H., Meng, Q.R., 1996. Three-dimensional architecture and dynamic analysis of the Qinling orogenic belt. *Sci. China (Series D)* 26, 1–6.
- Zhang, Z.Q., Zhang, G.W., Tang, S.H., Lu, X.X., 1999. Age of the Shahewan rapakivi granite in the Qinling Orogen, China, and its constraints on the end time of the main orogenic stage of this orogen. *Chin. Sci. Bull.* 44, 2001–2004.
- Zhang, G.W., Zhang, B.R., Yuan, X.C., Xiao, Q.H., 2001. Qinling Orogenic Belt and Continental Dynamics. Sci. Press, Beijing, pp. 1–806 (in Chinese).
- Zhang, C.L., Wang, T., Wang, X.X., 2008. Origin and tectonic setting of the Early Mesozoic granitoids in Qinling orogenic belt. *Geol. J. China Univ.* 14, 304–316.
- Zhang, H.F., Zhu, R.X., Santosh, M., Ying, J.F., Su, B.X., Hu, Y., 2013. Episodic widespread magma underplating beneath the North China Craton in the Phanerozoic: implications for craton destruction. *Gondwana Res.* 23 (1), 95–107.
- Zhao, D.P., Ohtani, E., 2009. Deep slab subduction and dehydration and their geodynamic consequences: evidence from seismology and mineral physics. *Gondwana Res.* 16, 401–413.
- Zhao, T.P., Zhai, M.G., Xia, B., Li, H.M., Zhang, Y.X., Wan, Y.S., 2004a. Study on the zircon SHRIMP ages of the Xionger Group volcanic rocks: constraint on the starting time of covering strata in the North China Craton. *Chin. Sci. Bull.* 9, 2495–2502.
- Zhao, Z.F., Zheng, Y.F., Wei, C.S., Wu, Y.B., 2004b. Zircon isotope evidence for recycling of subducted continental crust in post-collisional granitoids from the Dabie terrane in China. *Geophys. Res. Lett.* 31. <http://dx.doi.org/10.1029/2004GL021061>.
- Zhao, D.P., Maruyama, S., Omori, S., 2007a. Mantle dynamics of Western Pacific and East Asia: insight from seismic tomography and mineral physics. *Gondwana Res.* 11, 120–131.
- Zhao, Z.F., Zheng, Y.F., Wei, C.S., Wu, Y.B., 2007b. Post-collisional granitoids from the Dabie orogen in China: zircon U-Pb age, element and O isotope evidence for recycling of subducted continental crust. *Lithos* 93, 248–272.
- Zhao, G.C., He, Y.H., Sun, M., 2009. The Xionger volcanic belt at the southern margin of the North China Craton: petrographic and geochemical evidence for its outboard position in the Paleo-Mesoproterozoic Columbia Supercontinent. *Gondwana Res.* 16 (2), 170–181.
- Zhao, H.X., Jiang, S.Y., Frimmel, H.E., Dai, B.Z., Ma, L., 2012. Geochemistry, geochronology and Sr–Nd–Hf isotopes of two Mesozoic granitoids in the Xiaoqinling gold district: Implication for large-scale lithospheric thinning in the North China Craton. *Chem. Geol.* 294–295, 173–189.
- Zhao, J.H., Zhou, M.F., Zheng, J.P., 2013a. Constraints from zircon U-Pb ages, O and Hf isotopic compositions on the origin of Neoproterozoic peraluminous granitoids from the Jiangnan Fold Belt, South China. *Contrib. Miner. Petrol.* 166, 1505–1519.
- Zhao, J.H., Zhou, M.F., Zheng, J.P., Griffin, W., 2013b. Neoproterozoic tonalite and trondjemite in the Huangling complex, South China: Crustal growth and reworking in a continental arc environment. *Am. J. Sci.* 313, 540–583.
- Zheng, J.P., Griffin, W.L., O'Reilly, S.Y., Yu, C.M., Zhang, H.F., Pearson, N., Zhang, M., 2007. Mechanism and timing of lithospheric modification and replacement beneath the eastern North China Craton: peridotitic xenoliths from the 100 Ma Fuxin basalts and a regional synthesis. *Geochim. Cosmochim. Acta* 71, 5203–5225.
- Zheng, Y.F., Xiao, W.J., Zhao, G., 2013. Introduction to tectonics of China. *Gondwana Res.* 23 (4), 1189–1206.
- Zhou, H.W., Li, X.H., Zhong, Z.Q., Liu, Y., Xu, Q.D., 1997. Geochemistry of amphibolites within the Taihua complex from the Xiao Qinling area, western Henan and its tectonic implication. *Geochimica* 26, 87–100 (in Chinese with English abstract).
- Zhou, M.F., Chen, W.T., Wang, C.Y., Prevec, S.A., Liu, P.P.P., Howarth, G.H., 2013. Two stages of immiscible liquid separation in the formation of Panzhihua-type Fe-Ti-V oxide deposits, SW China. *Geosci. Front.* 4, 481–502.
- Zhu, G., Niu, M.L., Xie, C.L., Wang, Y.S., 2010. Sinistral to normal faulting along the tan-lu fault zone: evidence for geodynamic switching of the East China continental margin. *J. Geol.* 118, 277–293.
- Zhu, G., Jiang, D.Z., Zhang, B.L., Chen, Y., 2012a. Destruction of the eastern North China Craton in a backarc setting: evidence from crustal deformation kinematics. *Gondwana Res.* 22, 86–103.
- Zhu, X.Y., Chen, F.K., Liu, B.X., Siebel, W., 2012b. Zircon U-Pb and K-feldspar megacryst Rb–Sr isotopic ages and Sr–Hf isotopic composition of the Mesozoic Heyu pluton, eastern Qinling orogen, China. *Lithos* 156–159, 31–40.